

Published in final edited form as:

*Nat Immunol.* 2015 December ; 16(12): 1235–1244. doi:10.1038/ni.3290.

## Ectopic lymphoid structures function as microniches for tumor progenitor cells in hepatocellular carcinoma

Shlomi Finkin<sup>1,2</sup>, Detian Yuan<sup>3</sup>, Ilan Stein<sup>1,2</sup>, Koji Taniguchi<sup>4</sup>, Achim Weber<sup>5</sup>, Kristian Unger<sup>6</sup>, Jeffrey L. Browning<sup>7</sup>, Nicolas Goossens<sup>8,9</sup>, Shigeki Nakagawa<sup>8</sup>, Ganesh Gunasekaran<sup>10</sup>, Myron E. Schwartz<sup>10</sup>, Masahiro Kobayashi<sup>11</sup>, Hiromitsu Kumada<sup>11</sup>, Michael Berger<sup>1</sup>, Orit Pappo<sup>2</sup>, Klaus Rajewsky<sup>12</sup>, Yujin Hoshida<sup>8</sup>, Michael Karin<sup>4</sup>, Mathias Heikenwalder<sup>3,13</sup>, Yinon Ben-Neriah<sup>1</sup>, and Eli Pikarsky<sup>1,2</sup>

<sup>1</sup>Department of Immunology and Cancer Research, Institute for Medical Research Israel Canada (IMRIC), Hebrew University-Hadassah Medical School, Jerusalem 91120, Israel <sup>2</sup>Department of Pathology, Hadassah-Hebrew University Medical Center, Jerusalem 91120, Israel <sup>3</sup>Institute of Virology, Technische Universität München, Helmholtz Zentrum München, D-81675 Munich, Germany <sup>4</sup>Laboratory of Gene Regulation and Signal Transduction, Departments of Pharmacology and Pathology, School of Medicine, University of California, San Diego, 9500 Gilman Drive, MC 0723, La Jolla, CA 92093-0723, USA <sup>5</sup>Institute of Surgical Pathology, University and University-Hospital Zurich, CH-8091 Zurich, Switzerland <sup>6</sup>Research Unit of Radiation Cytogenetics, Helmholtz-Zentrum München, Ingolstädter-Landstrasse., D-85764 Neuherberg, Germany <sup>7</sup>Department of Microbiology, Boston University School of Medicine, Boston, MA 02118, USA <sup>8</sup>Division of Liver Diseases, Department of Medicine, Liver Cancer Program, Tisch Cancer Institute, Icahn School of Medicine at Mount Sinai, New York, USA <sup>9</sup>Division of Gastroenterology & Hepatology Geneva University Hospital, Switzerland <sup>10</sup>Recanati/ Miller Transplantation Institute, Icahn School of Medicine at Mount Sinai, New York, USA <sup>11</sup>Department of Hepatology, Toranomon Hospital, Tokyo, Japan <sup>12</sup>Max Delbrück Center for Molecular Medicine, 13092 Berlin, Germany <sup>13</sup>Division of Chronic Inflammation and Cancer, German Cancer Research Center (DKFZ) Heidelberg, 69120 Heidelberg, Germany

### Abstract

Ectopic lymphoid-like structures (ELS) are often observed in cancer, yet their function is obscure. Although ELSs signify good prognosis in certain malignancies, we found that hepatic ELSs indicate poor prognosis in hepatocellular carcinoma (HCC). We studied an HCC mouse model,

---

Users may view, print, copy, and download text and data-mine the content in such documents, for the purposes of academic research, subject always to the full Conditions of use:[http://www.nature.com/authors/editorial\\_policies/license.html#terms](http://www.nature.com/authors/editorial_policies/license.html#terms)

Correspondence: heikenwalder@helmholtz-muenchen.de (M.H), yinonb@ekmd.huji.ac.il (Y.B-N), peli@hadassah.org.il (E.P).

#### AUTHOR CONTRIBUTIONS

K.R., M.K., M.H., Y.B-N, E.P conceived the study; S.F, D.Y & I.S designed and carried out most experiments and data analysis; K.T, A.W, K.U, N.G, S.N, G.G, M.E.S, M.K, H.K, M.B & O.P carried out additional experiments, contributed samples and performed data analysis; J.L.B & K.R supplied novel reagents; S.F, D.Y, I.S, Y.H, M.K, M.H, Y.B-N & E.P wrote the manuscript.

#### ACCESSION CODES

Data for array CGH analysis are stored and available from ArrayExpress (<https://www.ebi.ac.uk/arrayexpress/>) accession number E-MTAB-3848.

#### COMPETING FINANCIAL INTERESTS

The authors declare competing financial interests: We have filed for a provisional patent related to this manuscript.

displaying abundant ELSs and found that they constitute immunopathological microniches, wherein progenitor malignant hepatocytes appear and thrive in a complex cellular and cytokine milieu until gaining self-sufficiency. Progenitor egression and tumor formation is associated with autocrine production of cytokines previously provided by the niche. ELSs develop upon cooperation between the innate and adaptive immune system which is facilitated by NF- $\kappa$ B activation and abolished by T cell depletion. These aberrant immune foci could be new targets for cancer therapy.

---

A central feature of tissue inflammation is the interaction between resident cells and immune cells. Cellular infiltration usually entails a diffuse influx of immune cells, scattered throughout the inflamed tissue. However, infiltrating leukocytes often form simple lymphoid aggregates or even more complex structures that histologically resemble lymphoid organs<sup>1, 2</sup>. These structures direct various B and T cell responses, possess organization of an appropriate microarchitecture and are referred to as ectopic lymphoid-like structures (ELS). ELSs often develop at sites of chronic inflammation where they influence the course of many diseases including distinct autoimmune, cardiovascular, metabolic and neurodegenerative diseases<sup>2</sup>. Although the presence of ELSs within inflamed tissues has been linked to both protective and deleterious outcomes in patients, the mechanisms governing ectopic lymphoid neogenesis in human pathology remain poorly defined. In cancer, for example, solid tumors such as colorectal, lung, breast and skin carcinomas, the presence of tumor-associated ELSs correlates with a better prognosis<sup>3, 4, 5, 6</sup>. It is believed that ELSs may coordinate endogenous antitumor immune responses that improve patient survival<sup>1, 5, 7</sup>. A role for ELSs in the premalignant phase of tumor growth has not been explored so far.

Hepatocellular carcinoma (HCC) is a major health problem, being the second leading cause of cancer-related deaths worldwide<sup>8</sup>. In most cases, human HCC is driven by chronic liver inflammation due to chronic viral hepatitis and non-alcoholic steatohepatitis (NASH)<sup>9, 10</sup>. Formation of hepatic ELSs is a prominent pathological hallmark of chronic viral infection<sup>11, 12</sup>, yet a functional role for these immune follicles in HCC pathogenesis has not been suggested or explored. Here we report that ELSs are associated with a poor prognosis in human HCC. Furthermore, we present a mouse model displaying abundant hepatic ELSs prior to the appearance of frank HCC nodules, for investigating the pathophysiological relationship between ELSs and tumor development. ELSs form cytokine rich microniches in which HCC progenitors thrive before gaining independence and moving out of the niches to form full blown HCCs. Interrupting ELS function abrogates HCC formation.

## RESULTS

### ELSs depend on NF- $\kappa$ B and signify poor prognosis in human HCC

To assess the relationship between hepatic ELS prevalence and prognosis in human HCC, we quantified the numbers of ELSs in the non-neoplastic liver parenchyma in a well-characterized cohort of 82 patients having undergone HCC resection, for which we had obtained clinical data, histological slides and gene expression data of the liver parenchyma<sup>13</sup>. ELS prevalence was histologically assessed in 66 cases (the subset of cases

with H&E-stained slides), using a published quantification scale<sup>14</sup> (Fig. 1a and Supplementary Fig. 1a). This analysis revealed that in contrast to colon, breast, lung and skin cancers<sup>3, 4, 5, 6</sup>, a high histological ELS score was associated with increased risk for late recurrence and a trend towards decreased overall survival after HCC resection (Supplementary Fig. 1b-d).

A 12-gene signature was shown to accurately assess the presence of ELSs in human tissues<sup>1</sup>. Using expression data available for these patients, we found a strong correlation between the histological ELS score and the 12 gene ELS signature (Fig. 1a,  $p < 0.001$ ), confirming its utility in the liver and enabling us to expand the analysis to include all 82 patients with transcriptome profiles. Fifteen out of 82 patients (18%) presented the ELS gene signature in the liver parenchyma (Fig. 1a), which was significantly associated with poor survival of HCC patients after curative surgical resection (Fig. 1b,  $p = 0.01$ ) and increased risk of late, but not early recurrence (Fig. 1c and Supplementary Fig. 1e;  $p = 0.03$  and  $p = 0.34$ , respectively). Of note, multivariable analysis showed that the ELS gene signature is an independent prognostic factor from the 186-gene prognostic - HCC risk gene signature previously identified in this cohort<sup>13</sup>, as well as the clinical prognostic staging system (Fig. 1d,e). Late recurrence, occurring 2 years after surgery, is considered to represent *de novo* carcinogenesis from the inflamed liver, while early recurrence occurring within 2 years of surgery results from dissemination of primary tumor cells<sup>15</sup>. Collectively, our clinical cohort analysis suggested that ELSs are associated with *de novo* HCC development in chronically inflamed and fibrotic or cirrhotic human livers.

The mechanisms underlying ELS formation in general and in cancer in particular are mostly obscure<sup>2, 16</sup>. To identify signaling pathways that could initiate or facilitate ELS development in HCC, we performed gene set enrichment analysis (GSEA) comparing gene expression in the liver parenchyma between patients with high vs. low ELS gene signatures. This analysis highlighted the interferon response and NF- $\kappa$ B signaling as top candidates (Supplementary Table 1). Further analysis of the correlation between activation of NF- $\kappa$ B signaling and hepatic ELSs using 3 different published NF- $\kappa$ B signatures confirmed the association for NF- $\kappa$ B (Fig. 1f and Supplementary Fig. 1f). These findings suggest that activation of the I kappa B kinase (IKK)-NF- $\kappa$ B signaling pathway could be an important mediator of hepatic ELS generation.

### Persistent IKK activation in hepatocytes induces ELSs

In order to examine the contribution of NF- $\kappa$ B signaling to generation of ELS and HCC, we developed an animal model. To activate the IKK-NF- $\kappa$ B signaling pathway in hepatocytes, we bred *R26Stop<sup>FL</sup>Ikk2ca* mice<sup>17</sup> with Albumin-cre (Alb-cre) mice<sup>18</sup>. The resulting IKK $\beta$ (EE)<sup>Hep</sup> mice express constitutively active IKK $\beta$ (EE) in hepatocytes (Fig. 2a) and show nuclear NF- $\kappa$ B and transcriptional activity comparable in their amounts to *Mdr2*<sup>-/-</sup> (also known as *Abcb4*<sup>-/-</sup>) mice, a model of chronic hepatitis<sup>19</sup>, but lower than TNF treated mice (Supplementary Fig. 2a-d), suggesting that IKK $\beta$ (EE)<sup>Hep</sup> mice display a level of innate immune activity which is similar to that present in common forms of chronic hepatitis. The livers of 3 month old IKK $\beta$ (EE)<sup>Hep</sup> mice lacked overt histopathology (Supplementary Fig. 2e). At 7 months IKK $\beta$ (EE)<sup>Hep</sup> mice revealed mild increases in liver macrophages, liver

damage markers and hepatocyte proliferation (Supplementary Fig. 2f-k). Importantly, multiple ELSs were apparent in livers of 7 month old  $IKK\beta(EE)^{Hep}$  mice, gradually growing in both size and number (Fig. 2b,c). Immunohistochemical staining revealed that ELSs were composed of T and B lymphocytes, neutrophils (located in the ELS periphery), NK cells, macrophages, T regulatory ( $T_{reg}$ ) cells, follicular dendritic cells and contained high endothelial venules, confirming that these were bona fide ELSs (Fig. 2d). We next analyzed ELSs present in the parenchyma of human livers with hepatitis (that were resected for HCC) and compared their immune cell composition to that of hepatic ELSs in  $IKK\beta(EE)^{Hep}$  mice. Histological analysis revealed that ELSs in  $IKK\beta(EE)^{Hep}$  mice were highly similar to their human counterparts (Fig. 2d). Flow cytometry of single cell suspensions of mouse ELSs confirmed the immunohistochemical analysis (Fig. 2e and Supplementary Fig. 2l,m). B and T lymphocyte compartmentalization, another characteristic feature of ELSs, was also observed in ELSs in  $IKK\beta(EE)^{Hep}$  mice and human hepatitis (Supplementary Fig. 2n). Furthermore, the ELS gene signature was significantly upregulated in liver parenchymas of  $IKK\beta(EE)^{Hep}$  mice compared to control Alb-cre mice (Supplementary Fig. 2o and Supplementary Table 2). Thus, persistent IKK activation in hepatocytes could be a key mediator of hepatic ELS formation in human hepatitis.

### Hepatic ELSs herald aggressive HCCs in $IKK\beta(EE)^{Hep}$ mice

At 20 months of age, 100% of  $IKK\beta(EE)^{Hep}$  mice developed HCC compared to 8% of control Alb-cre mice (Fig. 3a-c,  $p < 0.0001$ ). Histological analysis revealed that approximately half of  $IKK\beta(EE)^{Hep}$  tumors were well differentiated HCCs (WD-HCC); the remaining tumors were mixed cholangio-hepatocellular carcinomas (HCC-CCC, Fig. 3d), recognized by the presence of malignant glandular structures. Immunostaining for the HCC markers A6 and glutamine synthetase (GS), the proliferation marker Ki-67 and the matrix associated collagen IV (whose expression is downregulated in HCC), and the presence of metastases to lymph nodes and lungs confirmed that these were aggressive malignant HCCs (Supplementary Fig. 3a-c). Notably, mice harboring a single allele of  $IKK\beta(EE)$  showed decreased ELS number and size at 14 months (Supplementary Fig. 3d,e) followed by a similar decrease in HCC load at 20 months, when compared to mice harboring two such alleles (Supplementary Fig. 3f,g), underscoring an NF- $\kappa$ B dose-dependent ELS phenotype and an association between ELSs and HCC, respectively.

We also generated transgenic mice in which  $IKK\beta(EE)$  is driven by the Albumin promoter [Alb- $IKK\beta(EE)$  mice]. Of note, these mice also displayed ELSs and mild inflammation, followed with development of HCC (Supplementary Fig. 3h-j), corroborating the hepatocarcinogenic effect of constitutive  $IKK\beta(EE)$  expression in hepatocytes in a distinct mouse model. Treating  $IKK\beta(EE)^{Hep}$  mice with the hepatic carcinogen diethylnitrosamine (DEN) accelerated the appearance of ELSs (now appearing at 3 months), and HCCs (appearing at 9 months), without significantly altering their histological and molecular characteristics (Supplementary Fig. 3k-r).

Analysis of expression of a 16 gene set for assessing HCC aggressiveness<sup>20</sup>, revealed that HCCs from DEN-treated wild-type mice tended to cluster with wild-type livers, while HCCs from  $IKK\beta(EE)^{Hep}$  mice clustered with aggressive HCCs from transgenic mice

overexpressing *Myc* in hepatocytes together with germline deletion of *TP53* (*Myc-TP53*<sup>-/-</sup>, Fig. 3e, 7 out of 10 compared with 2 out of 20,  $p=0.002$ , Fisher's exact test). Tumors displaying the HCC-CCC morphology, which were only detected in the  $IKK\beta(EE)^{Hep}$  mice and not found in control DEN-treated ones, clustered with the more aggressive group (Fig. 3e). Of note, we could not detect a difference in the gene expression pattern between spontaneous and DEN induced HCCs in  $IKK\beta(EE)^{Hep}$  mice. Array comparative genomic hybridization (CGH) analyses of HCCs from DEN-treated Alb-cre control ( $n=12$ ), DEN-treated  $IKK\beta(EE)^{Hep}$  mice ( $n=11$ ) and 20-months old  $IKK\beta(EE)^{Hep}$  mice ( $n=13$ ) revealed chromosomal aberrations in all HCC samples, confirming their neoplastic nature. Data are stored and available from ArrayExpress (<https://www.ebi.ac.uk/arrayexpress/>) accession number E-MTAB-3848. Mixed HCC-CCC tumors were more complex than WD-HCC (Supplementary Fig. 3s). To validate the array CGH analysis, we prepared digital PCR probes directed at two genes, *Rgs2* and *Gab2*, targeting the two most common genomic amplifications. This analysis revealed a 90% concordance with results of the array CGH analysis. In addition, analysis of 13 additional  $IKK\beta(EE)^{Hep}$  HCCs revealed the presence of amplification of *Rgs2* gene copy number in 38% and amplification of *Gab2* gene copy number in 30% of the HCCs tested (Supplementary Fig. 3t). Taken together, these data confirmed that  $IKK\beta(EE)^{Hep}$  mice develop aggressive HCCs with a 100% penetrance.

### HCC progenitors first appear inside ELSs and later egress

Careful histological analysis revealed that the earliest malignant hepatocytes (noted at 3 and 7 months in DEN-treated and untreated  $IKK\beta(EE)^{Hep}$  mice, respectively), appeared first within newly-formed ELSs. These malignant hepatocytes were double positive for GFP (expressed from the hepatocyte specific *IKK\beta(EE)* transgene) and E-cadherin, confirming their hepatocyte origin and epithelial phenotype (Fig. 4a), and expressed multiple markers of HCC progenitors including A6, GP73 (GOLPH2), Sox9, CD44v6<sup>21</sup> and CK19 (Fig. 4b). At these earliest time points, HCC progenitors were largely found in ELSs and not elsewhere in the liver parenchyma (Supplementary Fig. 4a-c). GFP expression proved that these cells were derived from hepatocytes expressing the Alb-cre transgene (Supplementary Fig. 4d). These small clusters gradually grew, initially within ELSs and later on, migrating out to form visible tumors (Fig. 4c and Supplementary Fig. 4e). This histological sequence, of small groups of cells first appearing within ELSs, followed with gradual coalescence of groups of cells within the follicle boundary, which finally grew out into full-blown HCCs, was consistently seen in all  $IKK\beta(EE)^{Hep}$  mice of appropriate age in both spontaneous and DEN-treated groups (Supplementary Fig. 4f,g). To unequivocally prove the neoplastic nature of the epithelial cells that grew within the ELSs, we used laser capture micro-dissection to collect enriched populations of these cells. Indeed, 3 out of 11 lesions harbored amplification of *Rgs2* and 1 out of 11 harbored amplification of *Gab2* (Supplementary Fig. 4h), corroborating the neoplastic nature of these lesions and providing a genetic link between the malignant cells that were thriving within the ELSs and HCCs of  $IKK\beta(EE)^{Hep}$  mice.

Of note, several months after the first appearance of ELSs, we consistently observed clusters of malignant hepatocytes budding from the ELSs (Supplementary Fig. 4i). These clusters were either in continuity with or slightly separated from the intra-ELS malignant cells. To

better visualize the egression of clusters of malignant cells we co-immunostained serial sections with antibodies against CD44v6 (a marker for HCC progenitor cells<sup>21</sup>) and B220 and generated 3 dimensional reconstructions of ELSs. The resulting 3 dimensional representations clearly showed clusters of malignant cells budding out of ELSs (Fig. 4d and Supplementary video 1).

Although the IKK $\beta$ (EE) transgene is expressed throughout the parenchyma, ELSs are focal, suggesting that additional factors trigger ELS formation. Finding that ELS appearance was accelerated by DEN administration (Supplementary Fig. 3l,m) suggests that tissue damage could be of relevance, either by focal enhancement of hepatocyte NF- $\kappa$ B activation, or by triggering another cooperating pro-inflammatory pathway. To test this possibility we assessed the microanatomical localization of ELSs with respect to different liver zones. DEN is converted to its active metabolite in pericentral hepatocytes. Thus, if genotoxic stress is directly involved in formation of ELSs, the latter will be localized to pericentral regions. Immunostaining with GS (a marker of pericentral hepatocytes) revealed that ELSs were evenly distributed in the 3 liver zones in untreated IKK $\beta$ (EE)<sup>Hep</sup> mice; however, in DEN treated IKK $\beta$ (EE)<sup>Hep</sup> mice ELSs were almost entirely limited to the pericentral zone (Fig. 4e and Supplementary Fig. 4j,  $p < 0.0001$ ), suggesting a causal relationship between genotoxic stress and ELS formation.

To find out if HCC progenitors are also found in ELSs of human patients, we analyzed liver parenchyma from human livers resected for HCC. Triple immunofluorescence with antibodies against the human HCC markers HSP70 and SOX9 together with CK19 (which marks reactive ductular cells), revealed the presence of cells with HCC progenitor features within the human ELSs (Fig. 4f), attesting to a common ELS-related pathogenic mechanism in human HCC and the mouse model.

### Depletion of ELSs markedly attenuates murine HCC

The adaptive immune system is commonly considered a defense mechanism against cancer progression; accordingly human HCCs showing marked lymphocytic infiltration were found to have a better prognosis<sup>22</sup> and *Rag1*<sup>-/-</sup> mice, lacking an adaptive immune system, were shown to have more HCCs after DEN treatment<sup>23</sup>. Yet, despite its defense function, immune activation can result in various pathologies including cancer<sup>24, 25</sup>.

To test the functional role of ELSs in hepatocarcinogenesis, we bred IKK $\beta$ (EE)<sup>Hep</sup> mice with *Rag1*<sup>-/-</sup> mice which completely lack B and T cells. Consistent with a previous report<sup>23</sup>, there was a small increase in HCC numbers in DEN treated *Rag1*<sup>-/-</sup> mice (Fig. 5a-d). As expected, *Rag1* deletion in IKK $\beta$ (EE)<sup>Hep</sup> mice resulted in complete elimination of ELSs. However, in stark contrast with its pro-tumorigenic effect in *Rag1*<sup>-/-</sup> mice, loss of the adaptive immune system in IKK $\beta$ (EE)<sup>Hep</sup> -*Rag1*<sup>-/-</sup> mice dramatically attenuated hepatocarcinogenesis; most, if not all, of the pro-tumorigenic effect of the IKK $\beta$ (EE) transgene was lost in the absence of *Rag1* (Fig. 5a-d). Tumors that do develop in *Rag1*<sup>-/-</sup> IKK $\beta$ (EE)<sup>Hep</sup> mice were exclusively typical, WD-HCC and were negative for most HCC progenitors markers (Fig. 5e-g). Comparing proliferation, apoptosis and RelA (p65) nuclear accumulation between the HCCs in IKK $\beta$ (EE)<sup>Hep</sup> -*Rag1*<sup>-/-</sup> to well differentiated HCCs of IKK $\beta$ (EE)<sup>Hep</sup> mice did not reveal significant differences (Supplementary Fig. 5a-f), arguing

against a cell-autonomous effect of *Rag1* deficiency on HCC growth. Taken together these data suggest that generation of a focal immune microniche is dependent on a functional adaptive immune system and that the immune microniche promotes HCC.

To test whether ablation of ELS function after induction of tumors by DEN could still affect HCC formation in  $\text{IKK}\beta(\text{EE})^{\text{Hep}}$  mice, we administered anti-Thy1.2 antibody, to ablate T cells and potentially also innate lymphoid cells and NK cells which were also reported to respond to anti-Thy1.2 treatment, to mice between 18 to 30 weeks of age. Control mice received an isotype matched control antibody (Supplementary Fig. 6a). Immunostaining livers for CD3 confirmed almost complete T cell ablation (Fig. 6a). Indeed, anti-Thy1.2 treatment restricted ELS development (Fig. 6b), and markedly reduced HCC multiplicity and burden in  $\text{IKK}\beta(\text{EE})^{\text{Hep}}$  mice (Fig. 6c-e and Supplementary Fig. 6b-d). Thus, the adaptive immune system plays a strong pro-tumorigenic effect in  $\text{IKK}\beta(\text{EE})^{\text{Hep}}$  mice, which takes place after acquisition of the initiating tumor mutations.

### ELs express high amounts of growth promoting cytokines

We hypothesized that cytokines secreted by adaptive immune cells possibly present at high concentrations within ELs, could underlie their tumor-promoting effects. To identify pro-tumorigenic signals operative within ELs, we measured expression of multiple cytokines in liver parenchyma, ELs and HCCs from  $\text{IKK}\beta(\text{EE})^{\text{Hep}}$  mice and in human chronic viral hepatitis. Among others, Lymphotoxin (LT) family members, in particular  $\text{LT}\beta$  and LIGHT (also known as TNFSF14), and their downstream effectors, CCL17 and CCL20, were prominently overexpressed in human and mouse samples, along with signs of LT-driven non-canonical NF- $\kappa$ B pathway activation (Fig. 7a,b and Supplementary Fig. 7a-d).  $\text{LT}\beta$  is also expressed in ELs of patients with chronic hepatitis (Fig. 7b,c). Moreover, we noted a significant correlation between CCL17 and CCL20 mRNA expression and that of  $\text{LT}\beta$  in both human and mouse samples (Supplementary Fig. e-h). This suggests that Lymphotoxin  $\beta$  receptor ( $\text{LT}\beta\text{R}$ ) activation by  $\text{LT}\alpha$ ,  $\text{LT}\beta$  and/or LIGHT could play a key role in EL assembly and pro-tumorigenic processes<sup>26, 27, 28, 29</sup>.  $\text{LT}\beta\text{R}$  was reported to be expressed on hepatocytes, whereas  $\text{LT}\alpha$  and  $\text{LT}\beta$  are normally expressed in lymphocytes<sup>30</sup>. Indeed, mRNA *in situ* hybridization revealed that  $\text{LT}\beta$  mRNA was expressed in immune, but not epithelial cells in small ELs (Fig. 7d and Supplementary Fig. 7i). To identify the specific cell types which express  $\text{LT}\beta$ , we used flow sorting of single cell suspensions from ELs. This analysis revealed the  $\text{LT}\beta$  mRNA was expressed by both T and B lymphocytes, but not by hepatocytes (Supplementary Fig. 7j). However, in advanced large ELs, some of the neoplastic hepatocytes also expressed  $\text{LT}\beta$  and all full-blown HCCs always express  $\text{LT}\beta$  mRNA by histology (Fig. 7d and Supplementary Fig. 7i). Notably, when varying degrees of expression were noted in malignant hepatocytes within an EL,  $\text{LT}\beta$  mRNA expression occurred in malignant hepatocytes at the EL periphery, in particular within the egressing clusters (Fig. 7e,f and Supplementary Fig. 7k,l). This raised the hypothesis that immune cells within the ELs provide paracrine LT signals to early HCC progenitors, which are later replaced by an autocrine signal, allowing the malignant hepatocytes to gain independence from the niche. This presumption could be supported by the observation that transgenic overexpression of  $\text{LT}\alpha$  and  $\beta$  in hepatocytes was found to induce HCC<sup>26</sup>. Importantly, HCCs that developed in  $\text{IKK}\beta(\text{EE})^{\text{Hep}}$  mice under anti-Thy1.2-treatment and in  $\text{IKK}\beta(\text{EE})^{\text{Hep}}$  -

*Rag1*<sup>-/-</sup> livers showed marked reduction in *LTβ* mRNA expression, suggesting that exposure of tumor progenitors at early stages to niche-derived cytokines, renders them addicted to these cytokines, favoring acquisition of autocrine abilities to produce the same cytokines (Fig 7g,h and Supplementary Fig. 7m-p).

To test this hypothesis we blocked LT cytokines using a soluble *LTβR* fused to a murine immunoglobulin Fc portion (*LTβR-Ig*)<sup>26</sup>. Furthermore, to denote the time point of when LT blockade had the most efficient biologic effect, we subjected *IKKβ(EE)*<sup>Hep</sup> mice to three treatment regimens: 3-12 weeks of age, when *LTβ* is expressed by ELS immune cells; 13-22 weeks of age, when *LTβ* is expressed by both immune and malignant ELS cells; and 23-32 weeks of age during which *LTβ* is expressed similarly to the intermediate period, yet HCCs are more developed (Supplementary Fig. 8a,b). Measurements of expression of multiple cytokines in liver parenchyma showed reduction in many of the pro-inflammatory and of the LT-mediated cytokines (Fig. 8a). Of note, blocking LT signaling was associated with reduced NF-κB activation in ELS-residing malignant hepatocytes (Supplementary Fig. 8c,d), suggesting that LT signaling enhanced the low level of NF-κB activation induced by the *IKKβ(EE)* transgene. Remarkably, *LTβR-Ig* treatment in early and intermediate periods dramatically reduced HCC burden (Fig. 8b and Supplementary Fig. 8e,f). In contrast, *LTβR*-signaling inhibition at the late period resulted in a smaller, non-significant effect on HCC number and tumor volume. As LT inhibition proved ineffective in reducing tumorigenesis beyond 23 weeks of age, we hypothesized that the major inhibitory effect of LT-blockade could have been in ELSs where LT is primarily provided by the lymphocytes rather than in an autocrine manner by niche-external tumor cells. Indeed, histological inspection of early tumorigenesis stages in the late treatment group revealed a marked reduction in the number of intra-ELS HCC progenitors, and in both multiplicity and size of clusters of egressing cells (Fig. 8c,d and Supplementary Fig. 8g). This was associated with reduced proliferation of HCC progenitor cells in ELSs upon treatment (*CDC47*<sup>+</sup>*Sox9*<sup>+</sup> doubly-labeled cells, Fig. 8e-g), possibly accounting for a lower number of ELS-egressing atypical hepatocytes (Fig. 8c,d). It thus appears that paracrine LT stimulation within ELSs is a critical step in HCC development, amenable to anti-tumor intervention.

## DISCUSSION

Our study reveals a liver tumorigenesis program wherein specialized ELSs, associated with chronic NF-κB activation, foster atypical hepatocytes, that eventually acquire malignant properties. Importantly, our study indicates that ELSs - which are commonly present in human livers with HCC - promote rather than counteract tumor development as was previously demonstrated for several tumor types<sup>3, 4, 5, 6, 7</sup>. This highlights the existence of contrasting roles of ELSs in cancer that may be related to the different cancer types or perhaps reflect alternative phenotypes of ELSs. Shortly following ELS expansion and tumor progenitor egression, we observe distinct tumors carrying similar chromosomal aberrations, indicating that the tumors originated from ELS-nested atypical hepatocytes. The pro-tumorigenic effect of ELSs requires a competent adaptive immune system, providing lymphocyte-derived cytokines, supporting HCC progenitors until they are ready to egress out of their niches. Related hepatic ELSs are commonly found in chronic hepatitis patients who are at risk of developing HCC, ELSs might constitute a microniche for the population



of expanding HCC progenitor cells supporting cancer development. Similarly to our mouse models, these human follicles may form due to constitutive IKK activation by chronic hepatitis virus infection (e.g. HBV<sup>31</sup>, HCV<sup>32, 33</sup>). We may have therefore identified a critical window of immune-inflammatory action in tumor development, namely intra-niche growth of early tumor progenitors. The immune microniche environment appears to provide tumor progenitor cells with crucial survival and growth factors. Accordingly, preventing niche assembly or interfering with niche function significantly reduced HCC load in IKK $\beta$ (EE)<sup>Hep</sup> mice. ELSs are unique micro-anatomic structures which are commonly observed in multiple disease states, including cancer<sup>2</sup>. Specifically in the liver, ELSs are associated with chronic hepatitis<sup>11, 12, 34</sup>. The IKK $\beta$ (EE)<sup>Hep</sup> model provides for the first time functional information for ELSs, showing that they provide a unique microenvironment supporting growth of tumor progenitor cells. This notion is corroborated by our human studies showing a higher probability of late recurrence and death after HCC resection in patients with high hepatic ELS numbers. Of note, *late* recurrence, occurring 2 years after surgery, is considered to represent *de novo* carcinogenesis<sup>15</sup>.

Although our *Rag1*<sup>-/-</sup> experiments confirm previous studies showing that certain adaptive immune cells can play an anti-tumor role in hepatocarcinogenesis (i.e. in the absence of IKK-induced ELS formation), they reveal the dramatic pro-tumorigenic potential of adaptive immune cells in specific forms such as the ELS. An obvious difference between the pro- and anti-tumorigenic states is formation of highly structured microanatomic structures composed of hundreds of immune cells where the dominant effect is pro-tumorigenic. It is becoming clear that in lymphatic organs, three dimensional structures are key for shaping intercellular communication and cooperation among multiple immune cell types, frequently involving physical cell-cell interactions that are meticulously orchestrated to generate multiple effector mechanisms and bestow different phenotypes on the interacting cells<sup>35</sup>. Thus, the unique structure of the ELS as well as structural and composition changes over time could explain how the adaptive immune system turns from anti- to pro-tumorigenic. One obvious difference is that the compact structure of the ELS, grouping together high numbers of immune cells, likely suffices to generate a niche containing high concentrations of immune derived cytokines and growth factors providing a tumor-promoting environment.

Formation of ELSs is thought to depend on innate lymphoid cells (LTI) that are recruited to extranodal sites by chemoattracting cytokines<sup>2</sup>. The association between NF- $\kappa$ B activation in human livers and the 100% prevalence of ELSs in IKK $\beta$ (EE)<sup>Hep</sup> livers suggests that activation of hepatocyte NF- $\kappa$ B (known to occur in chronic hepatitis of diverse etiologies) plays a role in ELS formation in the liver, linking instigation of epithelial innate immunity and focal activation of adaptive immunity<sup>36</sup>. Although NF- $\kappa$ B is activated throughout the liver of IKK $\beta$ (EE)<sup>Hep</sup> mice, ELSs are focal, suggesting that additional cues are needed. Finding that ELS formation is significantly accelerated by DEN suggests that genotoxic stress could play a role in ELS formation. Supporting this notion is the different distribution of ELSs. In untreated IKK $\beta$ (EE)<sup>hep</sup> mice, ELSs are evenly distributed between liver zones, whereas in DEN treated mice, the ELSs are largely located in the pericentral zone where DEN is converted from a pro-carcinogen to a carcinogen that can attack DNA<sup>37</sup>. This joint activation of the NF- $\kappa$ B and DNA damage response pathways possibly generates a threshold level of cytokines that are sufficient to invoke the formation of ELSs. Of note, although a

previous report suggested that a persistently active IKK transgene expressed in hepatocytes did not lead to HCC induction<sup>38</sup>, it is plausible that either the expression level was not sufficiently high or that the follow up time was not long enough. Indeed, mice harboring a single allele of IKK $\beta$ (EE) show diminished tumor load compared with mice harboring two alleles, demonstrating that the level of expression of the transgene is important. Furthermore, we noted HCC development in two different IKK transgenic strains kept in different facilities.

Egression of tumor cells out of the niche where they first grew is a remarkable phenomenon observed in IKK $\beta$ (EE)<sup>hep</sup> mice. Seeds of cancer may germinate in an appropriate microenvironment, yet are capable of leaving the nursing niche and form full-blown malignant tumors only upon acquiring new capabilities. We speculate that acquisition of niche-independence is a hallmark prerequisite of solid tumors initiated within a supportive niche. One specific mechanism we detected in IKK $\beta$ (EE)<sup>hep</sup> mice is the acquisition of autocrine LT expression, but others are also very likely to take place. Recently, tumor progenitors were shown to respond to IL-6 from resident tissue macrophages, but later acquire autocrine IL-6 signaling that promotes malignant progression<sup>21</sup>. Identifying additional examples of immune-dependent tumor microniches, as well as their tumor progenitor support and egression mechanisms, might guide effective ways of arresting these processes for therapeutic purposes.

## METHODS

### Prognostic evaluation of histological ELSs, ELS gene signature, and NF- $\kappa$ B activation in liver tissues from curatively treated HCC patients

Prognostic association of the ELS gene signature was evaluated in genome-wide transcriptome profiles of cirrhotic liver tissues from 82 surgically-treated HCC patients followed for up to 15.6 years (median 7.8 years) reported in our previous study<sup>15</sup> (NCBI Gene Expression Omnibus accession number GSE10140). For each patient in the cohort, induction of the ELS gene signature was determined by Kolmogorov-Smirnov statistic-based gene set enrichment assessment<sup>39</sup> implemented in a custom analysis code written in R statistical language ([www.r-project.org](http://www.r-project.org)). Significance of the signature gene induction was determined as a prediction confidence p-value (significance threshold  $p < 0.05$ ) based on null distribution of the statistic generated by random permutation of the samples ( $n = 1,000$ ). Prognostic association of the ELS gene signature was assessed by Kaplan-Meier curves, log-rank test, and multivariable Cox regression modeling adjusted for the 186-gene prognostic/HCC risk signature we previously reported and clinical prognostic staging (American Association for Study of Liver Diseases [AASLD] staging system<sup>40</sup>). No clinical variables were associated with these clinical outcomes.

Correlation between presence of ELSs and NF- $\kappa$ B activation was determined by a modulation of 3 experimentally defined NF- $\kappa$ B target gene signatures in HeLa cells<sup>41</sup> and primary human fibroblasts and keratinocytes<sup>42</sup> and was evaluated in the same transcriptome dataset of 82 HCC patients. Histological ELS features were determined in 66 out of the 82 patients with H&E-stained slides as previously described: vague follicular aggregation (Agg), definite round-shaped cluster of small lymphocytes without germinal center (Fol),

and follicles with definite germinal centers composed of large lymphocytes with clear cytoplasm (GC)<sup>14</sup>. Each section was observed independently by two reviewers that were blinded to the patients' data. A consensus score was reached on a multi-head microscope in cases of discordance. Presence of histological ELS was defined as presence of any of the histological ELS features in 50% of portal areas for each patient.

### Human liver tissue

Human liver biopsy specimens were obtained from the archives of the Institute of Surgical Pathology, University Hospital Zurich (USZ), Switzerland and kept anonymous. The study protocol was approved by the ethical committee of the "GesundheitSEMirektion Kanton Zurich" (Ref. Nr. StV 26-2005 and KEK-ZH-Nr. 2013-0382) and was in accordance with the Helsinki declaration guidelines. Additional De-identified surgically resected human liver tissues were obtained via Mount Sinai Biorepository (IRB approval HS10-00135).

### Mice, HCC induction and anti-Thy1.2 and LT $\beta$ R-Ig treatments

All animal experiments were performed in accordance with the guidelines of the Hebrew University, University of California, San Diego (UCSD) and NIH for the use of animals for research. Previously described *ROSA26-LSL-IKK $\beta$ (EE)* mice<sup>17</sup> were bred with Albumin (Alb)-Cre mice<sup>18</sup> obtained from Jackson Laboratory (Bar Harbor, Maine, stock # 003574) to generate IKK $\beta$ (EE)<sup>Hep</sup> mice. Alb-cre mice served as controls for IKK $\beta$ (EE)<sup>Hep</sup> mice. Alb-IKK $\beta$ (EE) mice were generated at the transgenic mouse facility at UCSD as follows: HA-tagged IKK $\beta$ (EE) cDNA<sup>43</sup> was PCR-amplified and inserted into a plasmid containing 2.3 kb mouse Alb gene enhancer/promoter, rabbit  $\beta$ -globin second intron, rabbit  $\beta$ -globin polyadenylation signal and SV40 early gene polyadenylation signal (provided by Dr. K. Kohno, Nara Institute of Science and Technology, Nara, Japan)<sup>44</sup>. The expression cassette was excised, purified, and injected into fertilized C57BL/6 oocytes to generate founder mice, three of which transmitted the IKK $\beta$ (EE) transgene. *Rag1*<sup>-/-</sup> mice were purchased from Jackson Laboratory (stock # 002216), and *Mdr2*<sup>-/-</sup> mice have been described previously<sup>19</sup>. All mice were of a pure C57BL/6 genetic background and were bred and maintained in specific pathogen-free conditions. Only male mice were used. Animals were sacrificed by a lethal dose of anesthesia and perfused through the left ventricle with heparinized PBS followed by buffered formalin.

For hepatocarcinogenesis, mice were injected intraperitoneally (i.p) with 10 mg/kg DEN (Sigma) at 15 days of age. Mice were observed for development of tumors at 9 months of age. To inhibit LT $\beta$ R-signaling, a murine LT $\beta$ R: immunoglobulin G1 fusion protein (LT $\beta$ R-Ig, Biogen Idec), was used. Mice were i.p injected on a weekly basis with 100  $\mu$ g of LT $\beta$ R-Ig or MOPC21 (control murine-IgG1) for 10 consecutive weeks, starting either at 3 weeks of age (denoted early: 3-12), 13 weeks (intermediate: 13-22), or 23 weeks (late: 23-32). Mice were sacrificed at 33 weeks of age to evaluate HCC development (Supplementary Fig. 8a).

Anti Thy1.2 treatment: mice were injected IP every 2 days for 12 weeks with Thy1.2 antibody (BioXCell, catalog#: BE0066) or LTF-2 antibody for the control group (BioXCell, catalog#: BE0090). Mice were sacrificed at the age of 6.5 months.

*Myc-TP53*<sup>-/-</sup> liver tumors were kindly provided by Marie-Annick Buendia (Institut Pasteur, France). Briefly, woodchuck hepatitis virus (WHV)/*Myc* transgenic mice were mated with *p53*<sup>-/-</sup> mice to generate mice heterozygous for both the p53 mutation and the *Myc* transgene. The WHV/ *Myc p53*<sup>+delta</sup> mice spontaneously developed HCC, which frequently acquired a deletion of the remaining p53 allele. HCCs were further genotyped. *Myc-TP53*<sup>-/-</sup> HCCs were used as reference for a highly proliferative liver cancer in the 16-gene array analysis.

Serum alanine transaminase (ALT) and aspartate aminotransferase (AST) levels were determined using Reflotron Plus analysis system (Roche).

Examination of mouse H&E sections was performed by three expert liver pathologists (A.W, O.P. & E.P).

### Immunohistochemistry (IHC), Immunofluorescence and 3D reconstruction

Antibodies used were directed against: A6 (provided by Valentina Factor and Snorri Thorgeirsson, NIH, USA); B220 (BioLegend clone RA3-6B2); CD3 (Serotec clone CD3-12 or ZYTOMED, cat# RBK024); GFP (Invitrogen cat# A-11122); F4/80 (Serotec clone CI:A3-1); Ly-6G (BD Pharmingen, cat# 551459); FDC-M1 (BD Pharmingen clone # FDC-M1); Glutamine Synthetase (GS) (Abcam cat# ab16802); GP73/ GOLPH2 (Santa Cruz cat# sc-48011); Foxp3 (eBioscience clone FJK-16s); Ki67 (Thermo Scientific Clone SP6); CDC47 (MCM7) (Santa Cruz, cat# sc-56324); RelA (p65) NeoMarkers catalog #RB-1638); CD44 (eBioscience clone IM7); CD44(V6) (eBioscience clone 9A4); Sox9 (Santa Cruz cat# sc-20095); CK19 [hybridoma TROMA-III, deposited to Developmental Studies Hybridoma Bank (DSHB) by Kemler Rolf]; Collagen IV (Cedarlane Laboratories cat# CL50451AP); E-cadherin (BD clone 36/E-cadherin); Cleaved Caspase 3 (Cell Signaling cat# 9661). Antigen retrievals for B220, GFP, Ki67, CDC47, E-cadherin, RelA, Sox9, CK19 and Cleaved Caspase 3 were performed in 25mM citrate buffer pH 6.0; for GP73, Ly-6G, GS, Collagen IV, Foxp3, CD44, CD44(V6) and CD3 in EDTA buffer pH 8.0 (Invitrogen) – all by heating to 125°C for 3 min in decloaking chamber (Biocare Medical). Antigen retrieval for A6 and F4/80 was performed by incubation with 1mg/ml Pronase XXIV (Sigma). Immunofluorescence was performed on FFPE sections. Fluorophore conjugated secondary antibody used were Donkey anti-Mouse Cy5, Donkey anti-Rat Cy3 (Jackson Immunoresearch) and Alexa-Fluor Donkey anti-Goat 488 (life technologies). Hoechst 33342 (Invitrogen) was used as a nuclei marker.

Antibodies used for human sections were: CD3 (Cell Marque cat# 103A); CD15 (Biocare Medical, cat# CM029); CD20 (Cell Marque cat# 120R); CD23 (Novacastra Labs clone # 1B12); CD68 (Invitrogen clone KP1); Foxp3 (eBioscience clone # 236A/E7); HSP 70 (Santa Cruz, cat# sc-24) and LTβ (Biogen clone B27.B2). IHC staining of human sections was performed with BenchMark XT system (Ventana) using Cell Conditioning 1 (CC1, Ventana) for pretreatment, besides Foxp3 which was stained manually using EDTA buffer pH 8.0 (Invitrogen) for retrieval.

For quantification, stained slides were counted either manually by counting the number of positive cells per 10 high-power fields, or quantified with an Ariol SL-50 automated

scanning microscope and image-analysis system (Applied Imaging). Briefly, the frequency of positive cells was assessed with the appropriate module of the Ariol SL-50. For each sample, the percentage of positive cells or the intensity of the staining was determined in 10, arbitrary chosen, fields. Three dimensional reconstruction of ELSs in the liver was done using the  $\mu$ Core software (microDimensions GmbH, München, Germany) using a Mirax Midi Slide Scanner (Carl Zeiss microImaging GmbH, München, Germany) as described<sup>45</sup>.

### **Immunoblot (IB) and electrophoretic mobility shift assay (EMSA)**

Antibodies used for IB: Actin (Sigma clone AC-40); FLAG (Sigma clone Anti-Flag M2); p100/p52 (Cell Signaling cat #4882); RelB (Milipore cat # 06-1105); Tubulin (Sigma clone DM-1A). To prepare whole-cell lysates, tissues were lysed by mechanical grinding in RIPA buffer (50mM Tris-HCl pH 7.4, 150mM NaCl, 1mM EDTA, 1% NP-40 and 0.25% Na-deoxycholate) containing 1 $\times$  mixture of protease inhibitors (Sigma), 10mM Na<sub>3</sub>VO<sub>4</sub>, 10mM Na<sub>4</sub>P<sub>2</sub>O<sub>7</sub> and 50mM NaF. Total cell lysates were separated by SDS-PAGE and assessed by IB analysis, using sequential probing with the indicated primary Ab and an appropriate anti-IgG conjugated to HRP (Jackson). Immunoreactive bands were detected using ECL detection reagent (Pierce).

For EMSA, IRDye 700 labeled oligonucleotide (LI-COR Biosciences) corresponding to NF- $\kappa$ B specific consensus sequence was used. The binding reaction was performed using Odyssey Infrared electro-mobility shift assay kit (LI-COR Biosciences) according to the manufacturer protocol. Briefly, nuclear proteins were isolated from freshly isolated liver tissue using Cayman Nuclear Extraction Kit (Cayman Chemical Company) and total protein concentration was determined with the BCA Protein Assay Kit (Thermo Scientific). 20 ng of total nuclear protein was mixed with the labeled NF- $\kappa$ B oligonucleotide and left to bind for 30 minutes in the dark. Protein-DNA complexes were resolved by electrophoresis on 4% polyacrylamide Tris/Borate/EDTA (TBE) gel in the dark. Quantitative data was obtained using computerized densitometer and TINA software [version 2.07d (Raytest)].

### **RNA in-situ hybridization**

RNA in-situ hybridization was performed using the RNAscope 2.0 kit (Advanced Cell Diagnostics) according to manufacturer instructions. Briefly, 4  $\mu$ m FFPE sections were deparaffinized in xylene and pretreated to allow access of probe to target RNA. *LT $\beta$*  specific probe pairs (Advanced Cell Diagnostics) were hybridized to the target RNA at 40°C in a moist hybridization oven for 2 hours. The signal was amplified using AP-conjugated labeled probes, followed by colorimetric detection using Fast Red as substrate. *LT $\beta$*  mRNA was visualized using standard bright-field microscopy.

### **Array-based Comparative Genomic Hybridization (aCGH)**

Agilent oligonucleotide array based CGH for genomic DNA analysis of FFPE samples (Mouse Genome CGH Microarray 4x44K) was performed on genomic DNA extracted from FFPE liver tissues, according to the protocol provided by Agilent Technologies. Briefly, 500 ng of liver genomic DNA was differentially labeled with Cy3-dCTP (HCC) and Cy5-dCTP (liver tissue from C57BL/6 mice) by random primed labeling (CGH labeling kit for oligo array, Enzo Life Sciences). Liver genomic DNA from C57BL/6 mice was pooled and used

as reference DNA. After scanning the array slides, spot fluorescence intensities were extracted using the Feature Extraction Software (Agilent Technologies), and the raw data text files were used for further analysis. The data were imported into the R statistical platform (<http://www.R-project.org/>) and data quality outliers were filtered out using the quality flags as implemented in the Feature Extraction software, such as statistical population outliers or spots with foreground to background ratios smaller than 3. The  $\log_2$  ratios of each sample were collated into one matrix and preprocessed and analyzed as follows, using functions from the Bioconductor R package CGHcall<sup>46</sup>. Missing values were replaced using the values from neighboring probes by an imputation algorithm whereas probes with missing values in more than 30% of samples were excluded from the dataset. The remaining data were median normalized followed by breakpoint detection using a segmentation algorithm<sup>47</sup>, and the copy number status (loss, normal and gain) of each segment was determined using the CGHcall function<sup>46</sup>. The copy number calls of the single probes were transformed into copy number regions using the CGH regions package<sup>48</sup> and plotted for each chromosome according to their physical position.

### Proliferation/differentiation analysis of Figure 3e

The experimental group and tumor histology is indicated by the color code above each column. Clusters were determined by an unsupervised algorithm and designated A, B, the latter further subdivided into B1 and B2. Note that DEN induced HCCs from WT mice are more similar to WT liver parenchyma than IKK $\beta$ (EE)<sup>Hep</sup>, most of which fall into cluster B together with the aggressive *Myc-TP53*<sup>-/-</sup> mice. Statistical analyses of tumor types in the different clusters: DEN WD-HCCs vs. all IKK HCCs (cluster A vs. B)  $p < 0.0001$ ; DEN classic vs. IKK DEN tumors (both WD and HCC-CCC tumors) (A vs. B)  $p = 0.001$ ; DEN WD-HCCs vs. IKK spontaneous (spon) HCCs (both WD-HCCs and HCC-CCC tumors) (A vs. B)  $p = 0.04$ ; DEN WD-HCCs -IKK HCC-CCC (A vs. B)  $p = 0.006$ ; IKK WD-HCCs vs. IKK HCC-CCC (B1 vs. B2)  $p = 0.007$ . All  $p$  values were determined by two tailed chi-square test. Key: WT liver (purple)= parenchymal liver tissue from untreated 6 months old Alb-cre mice; DEN WD-HCC (green)= well differentiated HCCs from 9 months-old DEN-treated-Alb-cre mice; IKK spon. WD-HCC (blue)= well differentiated HCCs from 20 months-old IKK $\beta$ (EE)<sup>Hep</sup> mice; IKK spon. HCC-CCC (light brown)= undifferentiated mixed HCC-CCCs from 20 months-old IKK $\beta$ (EE)<sup>Hep</sup> mice; IKK DEN WD-HCC (yellow)= well differentiated HCCs from 9 months-old DEN-treated-IKK $\beta$ (EE)<sup>Hep</sup> mice; IKK DEN HCC-CCC (red)= undifferentiated mixed HCC-CCC from 9 months-old DEN-treated-IKK $\beta$ (EE)<sup>Hep</sup> mice; *Myc-TP53*<sup>-/-</sup> (brown): HCCs from the very aggressive mouse model for HCC, *Myc-TP53*<sup>-/-</sup> mice. See Supplementary Table 7 for primers sequence.

### FACS and cell sorter

ELs were dissected under binocular from IKK $\beta$ (EE)<sup>Hep</sup> livers and digested for 30 minutes in 500 $\mu$ l digestion buffer (HBSS with 0.2 mg/ml collagenase IV and 0.1 mg/ml DNase1) at 37°C with gentle agitation. The cells were strained through 40 $\mu$ m filter by washing with cold DMEM, centrifuged for 15 minutes, RBCs were lysed for 10 minutes at 25° with erythrocytes lysis buffer, washed again and resuspended in 0.5ml DMEM and kept on ice for a few hours until staining. Viability of isolated immune cells was around 85% as determined by Trypan blue. Cells were resuspended and stained in PBS supplemented with 1% fetal calf

serum and 1mM EDTA. Samples were stained and then analyzed by flow cytometry using a Gallios and Kaluza software (Beckman Coulter), or by fluorescence-activated cell sorter (FACS). Antibodies used for flow cytometry and FACS analysis: CD4 (clone RM-4.5, catalog#: 100536, BioLegend), CD8 (clone 53-6.7, catalog#: 65-0081 and 75-008, Tonbo), F4/80 (clone BM8, catalog#: 123127, BioLegend), CD11b (clone M1/70, catalog#: 101224, BioLegend), MHCII (clone KH74, catalog#: 115303, BioLegend), CD45.2 (clone 104, catalog#: 109807, BioLegend), NK1.1 (clone PK136, catalog#: 12-5941-83, eBioscience), TCR $\beta$  (clone: H57-597, catalog#: 35-5961, Tonbo), CD44 (clone IM7, catalog#: 103127, BioLegend), CD62L (clone MEL-14, catalog#: 104417, BioLegend), B220 (Catalog#: 553090, BD Pharmingen).

### Quantitative PCR analysis

Total RNA was extracted with Trizol (Invitrogen) and was reverse-transcribed by the high-capacity cDNA reverse transcription kit (Applied Biosystems). qPCR reactions were ran in triplicates in 384-well plates, and were carried out with SYBR green (Invitrogen) in 7900HT Fast Real-Time PCR System (Applied BioSystems). Results were analyzed using either the Dataassist 2.0 or qBase v1.3.5 softwares. HPRT and PPIA were used as reference genes in both human and murine analyses. Primer sequences are available in Supplementary Tables 3, 6 and 7 and expression fold and p-values in Supplementary Tables 2, 4 and 5.

### Digital PCR analysis

Genomic DNA was extracted from fresh frozen tissue with DNeasy (QIAGEN, Catalog# 69504) and from FFPE tissue with QIAamp DNA Micro Kit (QIAGEN, Catalog# 56304) and used for digital PCR analysis with the following TAQMAN probes: *Rgs2*, *Gab2* (Applied Biosystems, catalog# AB-4400291), *Tert* (Applied Biosystems, catalog# AB-4458368). High-throughput droplet digital PCR for quantitation of DNA copy number was done as described<sup>49</sup>.

### Statistical analysis

Results are expressed as mean  $\pm$  SEM. Statistical significance ( $p < 0.05$ ) was determined by either two-tailed Student's t-test, two tailed chi-square test or Fisher's exact test. For correlation analysis in mRNA expression levels, either Spearman or Pearson correlation tests at  $p < 0.05$  were used. Data was processed using Microsoft Excel or GraphPad Prism 6.0.

### Supplementary Material

Refer to Web version on PubMed Central for supplementary material.

### ACKNOWLEDGMENTS

We thank Einat Cinnamon, Marie-Annick Buendia, Kenji Kohno, Marc Ringelhan, Ruth Hillermann, Daniel Kull, Irit Gat-Viks, Yael Steuerman, Shalev Itzkovitz and Keren Bahar-Halpern for help and advice. Grant support: Dr. Miriam and Sheldon G. Adelson Medical Research Foundation (AMRF) to E.P & Y.B-N; European Research Council (ERC): LIVERMICROENV to E.P, PICH0 to Y.B-N and LiverCancerMechanism to M.H; Israel Science Foundation (ISF) to E.P, Y.B-N, I.S & O.P; Helmholtz alliance "preclinical comprehensive cancer center", Graduiertenkolleg (GRK482) to M.H; Krebsliga Schweiz (Oncosuisse) and Promedica Stiftung to A.W; NIH (CA118165; SRP ES010337; AI0043477) and the Hildyard chair for Mitochondrial and Metabolic Diseases to M.K; Japan Society for the Promotion of Science Postdoctoral Fellowships to K.T; NIH (DK099558), Irma T

Hirschl award and Dr. Harold and Golden Lamport award to Y.H; the FLAGS foundation to N.G.; the Uehara memorial foundation to S.N.

## REFERENCES

1. Coppola D, Nebozhyn M, Khalil F, Dai H, Yeatman T, Loboda A, et al. Unique ectopic lymph node-like structures present in human primary colorectal carcinoma are identified by immune gene array profiling. *Am J Pathol.* 2011; 179(1):37–45. [PubMed: 21703392]
2. Pitzalis C, Jones GW, Bombardieri M, Jones SA. Ectopic lymphoid-like structures in infection, cancer and autoimmunity. *Nat Rev Immunol.* 2014; 14(7):447–462. [PubMed: 24948366]
3. Di Caro G, Bergomas F, Grizzi F, Doni A, Bianchi P, Malesci A, et al. Occurrence of tertiary lymphoid tissue is associated with T-cell infiltration and predicts better prognosis in early-stage colorectal cancers. *Clinical cancer research: an official journal of the American Association for Cancer Research.* 2014; 20(8):2147–2158. [PubMed: 24523438]
4. Dieu-Nosjean MC, Antoine M, Danel C, Heudes D, Wislez M, Poulot V, et al. Long-term survival for patients with non-small-cell lung cancer with intratumoral lymphoid structures. *Journal of clinical oncology: official journal of the American Society of Clinical Oncology.* 2008; 26(27):4410–4417. [PubMed: 18802153]
5. Gu-Trantien C, Loi S, Garaud S, Equeter C, Libin M, de Wind A, et al. CD4(+) follicular helper T cell infiltration predicts breast cancer survival. *J Clin Invest.* 2013; 123(7):2873–2892. [PubMed: 23778140]
6. Messina JL, Fenstermacher DA, Eschrich S, Qu X, Berglund AE, Lloyd MC, et al. 12-Chemokine gene signature identifies lymph node-like structures in melanoma: potential for patient selection for immunotherapy? *Scientific reports.* 2012; 2:765. [PubMed: 23097687]
7. Di Caro G, Marchesi F. Tertiary lymphoid tissue: A gateway for T cells in the tumor microenvironment. *Oncoimmunology.* 2014; 3:e28850. [PubMed: 25083321]
8. Stewart, BW.; Wild, CPe. *World Cancer Report 2014.* 2014.
9. El-Serag HB. Hepatocellular carcinoma. *The New England journal of medicine.* 2011; 365(12):1118–1127. [PubMed: 21992124]
10. Umemura A, Park EJ, Taniguchi K, Lee JH, Shalapour S, Valasek MA, et al. Liver damage, inflammation, and enhanced tumorigenesis after persistent mTORC1 inhibition. *Cell Metab.* 2014; 20(1):133–144. [PubMed: 24910242]
11. Scheuer PJ, Ashrafzadeh P, Sherlock S, Brown D, Dusheiko GM. The pathology of hepatitis C. *Hepatology.* 1992; 15(4):567–571. [PubMed: 1551631]
12. Gerber MA. Histopathology of HCV infection. *Clin Liver Dis.* 1997; 1(3):529–541. vi. [PubMed: 15560056]
13. Hoshida Y, Villanueva A, Kobayashi M, Peix J, Chiang DY, Camargo A, et al. Gene expression in fixed tissues and outcome in hepatocellular carcinoma. *The New England journal of medicine.* 2008; 359(19):1995–2004. [PubMed: 18923165]
14. Murakami J, Shimizu Y, Kashii Y, Kato T, Minemura M, Okada K, et al. Functional B-cell response in intrahepatic lymphoid follicles in chronic hepatitis C. *Hepatology.* 1999; 30(1):143–150. [PubMed: 10385650]
15. Hoshida Y, Villanueva A, Llovet JM. Molecular profiling to predict hepatocellular carcinoma outcome. *Expert review of gastroenterology & hepatology.* 2009; 3(2):101–103. [PubMed: 19351279]
16. Drayton DL, Liao S, Mounzer RH, Ruddle NH. Lymphoid organ development: from ontogeny to neogenesis. *Nat Immunol.* 2006; 7(4):344–353. [PubMed: 16550197]
17. Sasaki Y, Derudder E, Hobeika E, Pelanda R, Reth M, Rajewsky K, et al. Canonical NF-kappaB activity, dispensable for B cell development, replaces BAFF-receptor signals and promotes B cell proliferation upon activation. *Immunity.* 2006; 24(6):729–739. [PubMed: 16782029]
18. Postic C, Magnuson MA. DNA excision in liver by an albumin-Cre transgene occurs progressively with age. *Genesis.* 2000; 26(2):149–150. [PubMed: 10686614]



19. Pikarsky E, Porat RM, Stein I, Abramovitch R, Amit S, Kasem S, et al. NF-kappaB functions as a tumour promoter in inflammation-associated cancer. *Nature*. 2004; 431(7007):461–466. [PubMed: 15329734]
20. Cairo S, Armengol C, De Reynies A, Wei Y, Thomas E, Renard CA, et al. Hepatic stem-like phenotype and interplay of Wnt/beta-catenin and Myc signaling in aggressive childhood liver cancer. *Cancer Cell*. 2008; 14(6):471–484. [PubMed: 19061838]
21. He G, Dhar D, Nakagawa H, Font-Burgada J, Ogata H, Jiang Y, et al. Identification of liver cancer progenitors whose malignant progression depends on autocrine IL-6 signaling. *Cell*. 2013; 155(2): 384–396. [PubMed: 24120137]
22. Wada Y, Nakashima O, Kutami R, Yamamoto O, Kojiro M. Clinicopathological study on hepatocellular carcinoma with lymphocytic infiltration. *Hepatology*. 1998; 27(2):407–414. [PubMed: 9462638]
23. Schneider C, Teufel A, Yevsa T, Staib F, Hohmeyer A, Walenda G, et al. Adaptive immunity suppresses formation and progression of diethylnitrosamine-induced liver cancer. *Gut*. 2012; 61(12):1733–1743. [PubMed: 22267597]
24. Okin D, Medzhitov R. Evolution of inflammatory diseases. *Curr Biol*. 2012; 22(17):R733–740. [PubMed: 22975004]
25. Karin M, Lawrence T, Nizet V. Innate immunity gone awry: linking microbial infections to chronic inflammation and cancer. *Cell*. 2006; 124(4):823–835. [PubMed: 16497591]
26. Haybaeck J, Zeller N, Wolf MJ, Weber A, Wagner U, Kurrer MO, et al. A lymphotoxin-driven pathway to hepatocellular carcinoma. *Cancer Cell*. 2009; 16(4):295–308. [PubMed: 19800575]
27. Wolf MJ, Seleznik GM, Heikenwalder M. Lymphotoxin's link to carcinogenesis: friend or foe? from lymphoid neogenesis to hepatocellular carcinoma and prostate cancer. *Advances in experimental medicine and biology*. 2011; 691:231–249. [PubMed: 21153327]
28. Tumanov AV, Koroleva EP, Christiansen PA, Khan MA, Ruddy MJ, Burnette B, et al. T cell-derived lymphotoxin regulates liver regeneration. *Gastroenterology*. 2009; 136(2):694–704. e694. [PubMed: 18952083]
29. Drutskaya MS, Efimov GA, Kruglov AA, Kuprash DV, Nedospasov SA. Tumor necrosis factor, lymphotoxin and cancer. *IUBMB life*. 2010; 62(4):283–289. [PubMed: 20155809]
30. Bauer J, Namineni S, Reisinger F, Zoller J, Yuan D, Heikenwalder M. Lymphotoxin, NF-kB, and cancer: the dark side of cytokines. *Dig Dis*. 2012; 30(5):453–468. [PubMed: 23108301]
31. Yun C, Um HR, Jin YH, Wang JH, Lee MO, Park S, et al. NF-kappaB activation by hepatitis B virus X (HBx) protein shifts the cellular fate toward survival. *Cancer letters*. 2002; 184(1):97–104. [PubMed: 12104053]
32. Yu GY, He G, Li CY, Tang M, Grivennikov S, Tsai WT, et al. Hepatic Expression of HCV RNA-Dependent RNA Polymerase Triggers Innate Immune Signaling and Cytokine Production. *Mol Cell*. 2012
33. Arzumanyan A, Reis HM, Feitelson MA. Pathogenic mechanisms in HBV- and HCV-associated hepatocellular carcinoma. *Nature reviews Cancer*. 2013; 13(2):123–135. [PubMed: 23344543]
34. Mosnier JF, Degott C, Marcellin P, Henin D, Erlinger S, Benhamou JP. The intraportal lymphoid nodule and its environment in chronic active hepatitis C: an immunohistochemical study. *Hepatology*. 1993; 17(3):366–371. [PubMed: 8444410]
35. Qi H, Kastenmuller W, Germain RN. Spatiotemporal basis of innate and adaptive immunity in secondary lymphoid tissue. *Annu Rev Cell Dev Biol*. 2014; 30:141–167. [PubMed: 25150013]
36. Iwasaki A, Medzhitov R. Regulation of adaptive immunity by the innate immune system. *Science*. 2010; 327(5963):291–295. [PubMed: 20075244]
37. Verna L, Whysner J, Williams GM. N-nitrosodiethylamine mechanistic data and risk assessment: bioactivation, DNA-adduct formation, mutagenicity, and tumor initiation. *Pharmacol Ther*. 1996; 71(1-2):57–81. [PubMed: 8910949]
38. Yau TO, Chan CF, Gee-San Lam S, Cheung OF, Ching YP, Jin DY, et al. Hepatocyte-specific activation of NF-kappaB does not aggravate chemical hepatocarcinogenesis in transgenic mice. *J Pathol*. 2009; 217(3):353–361. [PubMed: 19090486]
39. Subramanian A, Tamayo P, Mootha VK, Mukherjee S, Ebert BL, Gillette MA, et al. Gene set enrichment analysis: a knowledge-based approach for interpreting genome-wide expression

- profiles. *Proceedings of the National Academy of Sciences of the United States of America*. 2005; 102(43):15545–15550. [PubMed: 16199517]
40. Bruix J, Sherman M, American Association for the Study of Liver D. Management of hepatocellular carcinoma: an update. *Hepatology*. 2011; 53(3):1020–1022. [PubMed: 21374666]
41. Tian B, Nowak DE, Jamaluddin M, Wang S, Brasier AR. Identification of direct genomic targets downstream of the nuclear factor-kappaB transcription factor mediating tumor necrosis factor signaling. *The Journal of biological chemistry*. 2005; 280(17):17435–17448. [PubMed: 15722553]
42. Hinata K, Gervin AM, Jennifer Zhang Y, Khavari PA. Divergent gene regulation and growth effects by NF-kappa B in epithelial and mesenchymal cells of human skin. *Oncogene*. 2003; 22(13):1955–1964. [PubMed: 12673201]
43. Delhase M, Hayakawa M, Chen Y, Karin M. Positive and negative regulation of IkappaB kinase activity through IKKbeta subunit phosphorylation. *Science*. 1999; 284(5412):309–313. [PubMed: 10195894]
44. Saito M, Iwawaki T, Taya C, Yonekawa H, Noda M, Inui Y, et al. Diphtheria toxin receptor-mediated conditional and targeted cell ablation in transgenic mice. *Nat Biotechnol*. 2001; 19(8):746–750. [PubMed: 11479567]
45. Huang LR, Wohlleber D, Reisinger F, Jenne CN, Cheng RL, Abdullah Z, et al. Intrahepatic myeloid-cell aggregates enable local proliferation of CD8(+) T cells and successful immunotherapy against chronic viral liver infection. *Nat Immunol*. 2013; 14(6):574–583. [PubMed: 23584070]
46. van de Wiel MA, Kim KI, Vosse SJ, van Wieringen WN, Wilting SM, Ylstra B. CGHcall: calling aberrations for array CGH tumor profiles. *Bioinformatics*. 2007; 23(7):892–894. [PubMed: 17267432]
47. Venkatraman ES, Olshen AB. A faster circular binary segmentation algorithm for the analysis of array CGH data. *Bioinformatics*. 2007; 23(6):657–663. [PubMed: 17234643]
48. van de Wiel MA, Wieringen WN. CGHregions: dimension reduction for array CGH data with minimal information loss. *Cancer informatics*. 2007; 3:55–63. [PubMed: 19455235]
49. Hindson BJ, Ness KD, Masquelier DA, Belgrader P, Heredia NJ, Makarewicz AJ, et al. High-throughput droplet digital PCR system for absolute quantitation of DNA copy number. *Anal Chem*. 2011; 83(22):8604–8610. [PubMed: 22035192]

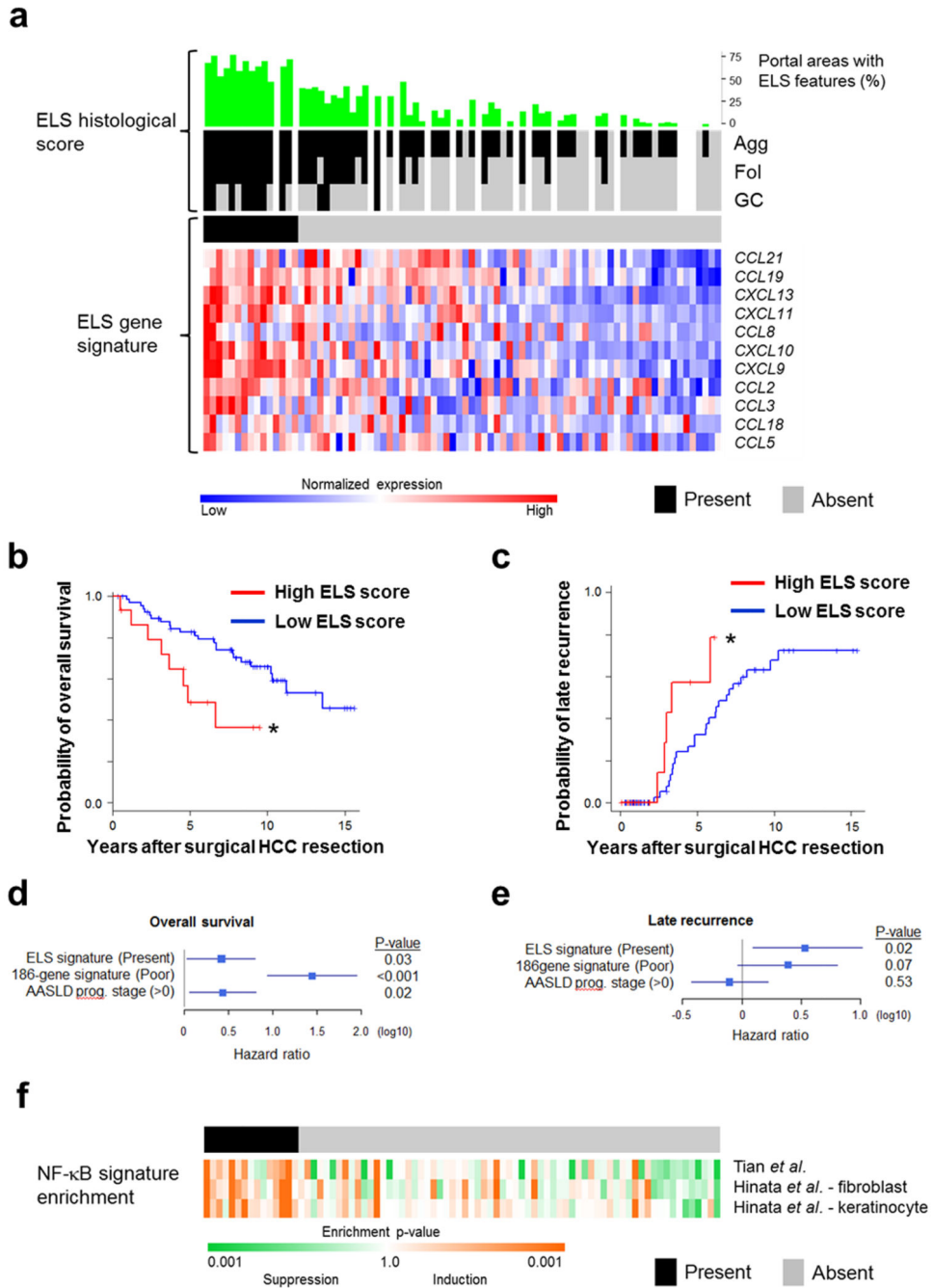


**Figure 1. Hepatic ELSs signify a poor prognosis in human HCC and are associated with NF-κB activation**

(a) Upper panel, histological ELS score: For each human sample (n=82) the percentage of portal areas with ELS features (green) and the type of ELS was evaluated histologically (black and grey colors indicate presence and absence of histological ELS, respectively; Agg= Aggregate, Fol=Follicle, GC=Germinal Center). Gaps indicate lack of H&E-stained slides. Lower panel, ELS gene signature: Heatmap for expression of each of the 12 genes composing the ELS gene signature<sup>6</sup>. Presence of high ELS gene signature is shown in the

black color bar above the gene expression heatmap. Presence of high ELS gene signature was determined by coherent overexpression of the signature genes with statistical significance (prediction confidence  $p < 0.05$ ), as described in the Methods (black – present, grey – absent; upper horizontal bar). Cases in upper and lower panels are ordered according to ELS gene signature. **(b,c)** Kaplan Meier curves for survival (b) or late recurrence (c) after resection of HCC, in patients with high (red) and low (blue) ELS gene signatures in the liver parenchyma [n=82 patients (15 high score, 67 low score); \* $p=0.01$  and  $0.03$  for (b) and (c), respectively, Log-rank test]. **(d,e)** Hazard ratios of the ELS gene signature for overall survival (d) and late recurrence (e) in multivariable Cox regression modeling adjusted for 186-gene prognostic HCC risk<sup>13</sup> and American Association for Study of Liver Diseases (AASLD) prognostic stage<sup>40</sup>. Bars - 95% confidence interval. **(f)** Heatmap for NF- $\kappa$ B signature enrichment in the same cohort of human patients as in (a). NF- $\kappa$ B signature enrichment was determined by modulation of 3 experimentally defined sets in HeLa cells, primary human fibroblasts and keratinocytes (see **Methods** for details). In all 3 panels, samples are ordered according to the extent of ELS signature induction from left to right (same order as in a).

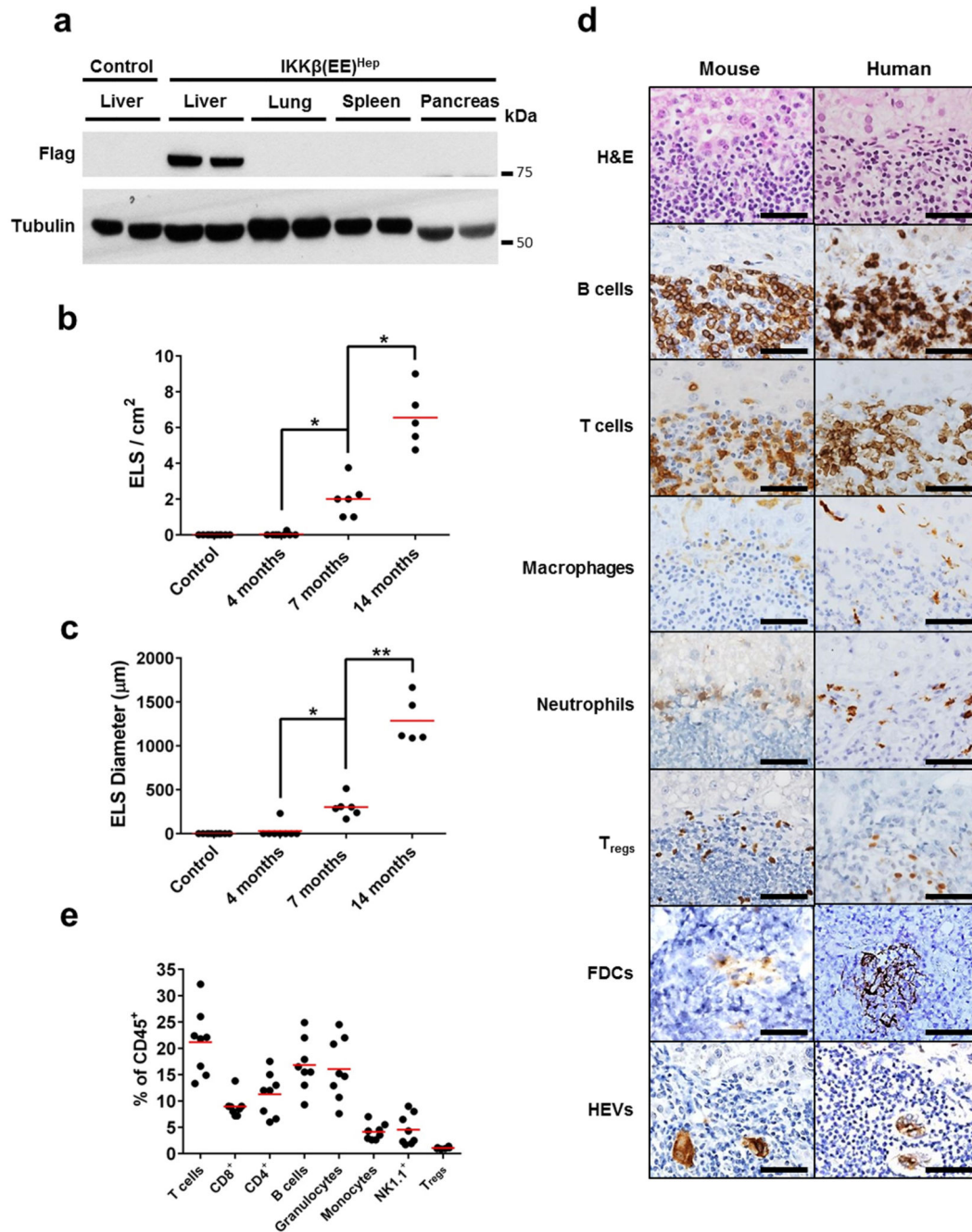


**Figure 2. Persistent liver IKK activation induces ectopic lymphoid structures**

(a) Immunoblot analysis for Flag-tagged IKKβ(EE) in tissues of Alb-cre control and IKKβ(EE)<sup>Hep</sup> mice. Tubulin - loading control (shown two representative mice per group). (b,c) Quantification of ELS number and size in IKKβ(EE)<sup>Hep</sup> livers. Control Alb-cre mice do not develop follicles (n=10,8,6,5 for control, 4,7 and 14 months old IKKβ(EE)<sup>Hep</sup> mice, respectively; \*p=0.0002, \*\*p=0.00001, two-tailed Students t-test, red line signifies mean). (d) Representative H&E and immunostained sections of IKKβ(EE)<sup>Hep</sup> mouse and human livers from patients with chronic hepatitis showing presence of immune follicles (scale bars

50  $\mu\text{m}$ , FDCs, follicular dendritic cells, HEVs, high endothelial venules). **(e)** Cells from microscopically isolated ELSs from  $\text{IKK}\beta(\text{EE})^{\text{Hep}}$  mice livers were analyzed by flow cytometry for markers indicative of the shown cell types (red line signifies mean, results are representative of ELSs isolated from at least 6  $\text{IKK}\beta(\text{EE})^{\text{Hep}}$  mice). Data are representative of three independent experiments in (a) and (d) and of one experiment in (e).

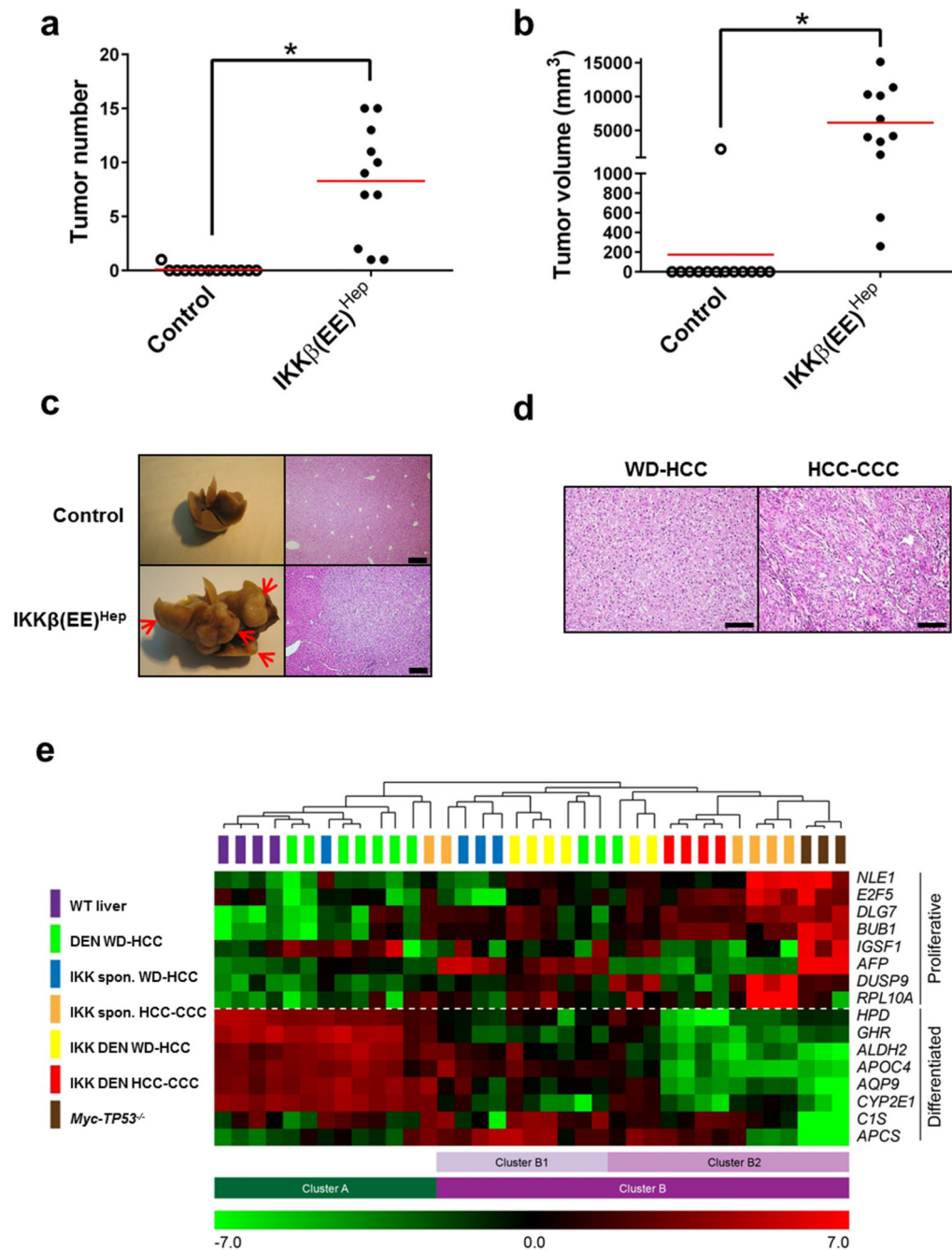


**Figure 3. Persistent activation of IKK in hepatocytes induces aggressive HCC**  
**(a,b)** Tumor number ( > 0.5 cm) and volume in livers of 20-month-old Alb-cre control and IKK $\beta$ (EE)<sup>Hep</sup> mice (n=13,11 for control and IKK $\beta$ (EE)<sup>Hep</sup>, respectively; \*p 0.0002, two-tailed Students t-test, red line signifies mean). **(c)** Representative livers and H&E stained sections from 20-month-old Alb-cre and IKK $\beta$ (EE)<sup>Hep</sup> mice. Arrows indicate tumors (scale bar= 200  $\mu$ m). **(d)** Representative H&E stains of HCCs from 20-month old IKK $\beta$ (EE)<sup>Hep</sup> mice. WD-HCC= well-differentiated HCC, CCC= cholangiocellular carcinoma (scale bar= 100  $\mu$ m). **(e)** Heat map representation of relative mRNA expression of a 16-gene HCC

proliferation and differentiation signature<sup>20</sup> in wild-type (WT) liver parenchyma or HCCs derived from the indicated mice (for further details see **Methods**). Clusters were determined by an unsupervised algorithm and designated A, B, the latter further subdivided into B1 and B2. Note that DEN induced HCCs from WT mice are more similar to WT liver parenchyma than IKK $\beta$ (EE)<sup>Hep</sup>, most of which fall into cluster B together with the aggressive HCCs of *Myc-TP53*<sup>-/-</sup> mice. Statistical analyses of tumor types in the different clusters: DEN WD-HCCs vs. all IKK HCCs (cluster A vs. B)  $p=6.0E-05$ ; DEN WD vs. IKK DEN tumors (both WD and HCC-CCC tumors) (A vs. B)  $p=0.001$ ; DEN WD-HCCs vs. IKK spontaneous (spon) HCCs (both WD-HCCs and HCC-CCC tumors) (A vs. B)  $p=0.04$ ; DEN WD-HCCs - IKK HCC-CCC (A vs. B)  $p=0.006$ ; IKK WD-HCCs vs. IKK HCC-CCC (B1 vs. B2)  $p=0.007$ .  $n=4,7,8,8,3$  for WT, DEN treated Alb-cre, DEN treated IKK $\beta$ (EE)<sup>Hep</sup>, untreated IKK $\beta$ (EE)<sup>Hep</sup> and *Myc-TP53*<sup>-/-</sup> mice, respectively; All  $p$  values were determined by two tailed chi-square test. Data are representative of two independent experiments in (a) and (b) and of one experiment in (e).



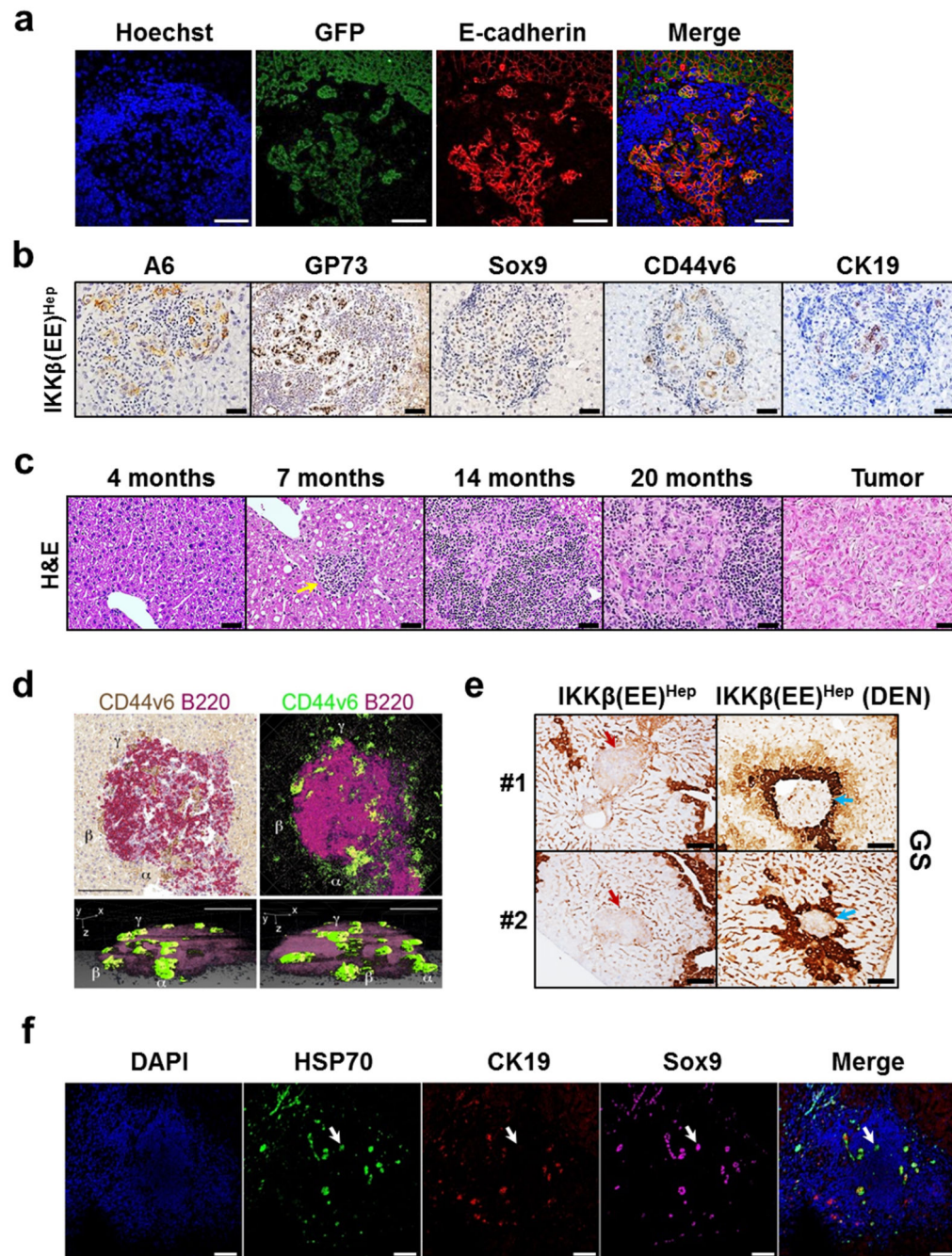


**Figure 4. HCC progenitors appear in ELSs and progressively egress out**

**a)** Representative co-immunofluorescence stains for GFP (green) expressed from the hepatocyte specific IKK $\beta$ (EE) transgene and the epithelial marker E-cadherin (red) depicting the epithelial origin of HCC progenitors. Hoechst 33342 (blue) marks the nuclei (scale bars 100  $\mu$ m). **(b)** Representative immunostains for indicated HCC progenitor markers in ELSs of IKK $\beta$ (EE)<sup>Hep</sup> mice (scale bars 50  $\mu$ m). **(c)** Representative H&E stained sections of IKK $\beta$ (EE)<sup>Hep</sup> livers depicting ELS to HCC progression (arrow points to small ELS; scale bars 50  $\mu$ m). **(d)** Representative 3-dimensional (3D) reconstruction of an ELS from a 6

month old DEN-treated  $\text{IKK}\beta(\text{EE})^{\text{Hep}}$  mouse. Left upper panel: double color immunostaining for CD44v6 (brown) and B220 (red). Right upper panel: color conversion of the left panel (brown to green, red to purple). Lower panels: Two different rotations of a 3D reconstruction. Note green  $\text{CD44v6}^+$  progenitor cells egressing out of the ELS at multiple points (scale bars 100  $\mu\text{m}$ ).  $\alpha$ ,  $\beta$  and  $\gamma$  show the same region in all panels. See also Supplementary video 1. **(e)** Representative immunostains of two different livers (#1 and #2) from 14 month old untreated  $\text{IKK}\beta(\text{EE})^{\text{Hep}}$  mice and 6 month old DEN treated  $\text{IKK}\beta(\text{EE})^{\text{Hep}}$  mice for the pericentral marker glutamine synthetase (GS). Red and blue arrows indicate periportal and pericentral ELSs, respectively. Brown staining highlights pericentral zones (scale bars 100  $\mu\text{m}$ ). **(f)** Representative confocal microscopy images of ELS-containing liver sections from a human patient for the HCC progenitor markers HSP70 (green) and Sox9 (purple) and for the bile duct marker CK19 (red). DAPI (blue) marks the nuclei. Arrow points to a group of HCC progenitors (scale bars 100  $\mu\text{m}$ , arrow points to progenitor cell). Data are representative of three independent experiments in (a) and (b), and of one experiment in (d), (e) and (f).

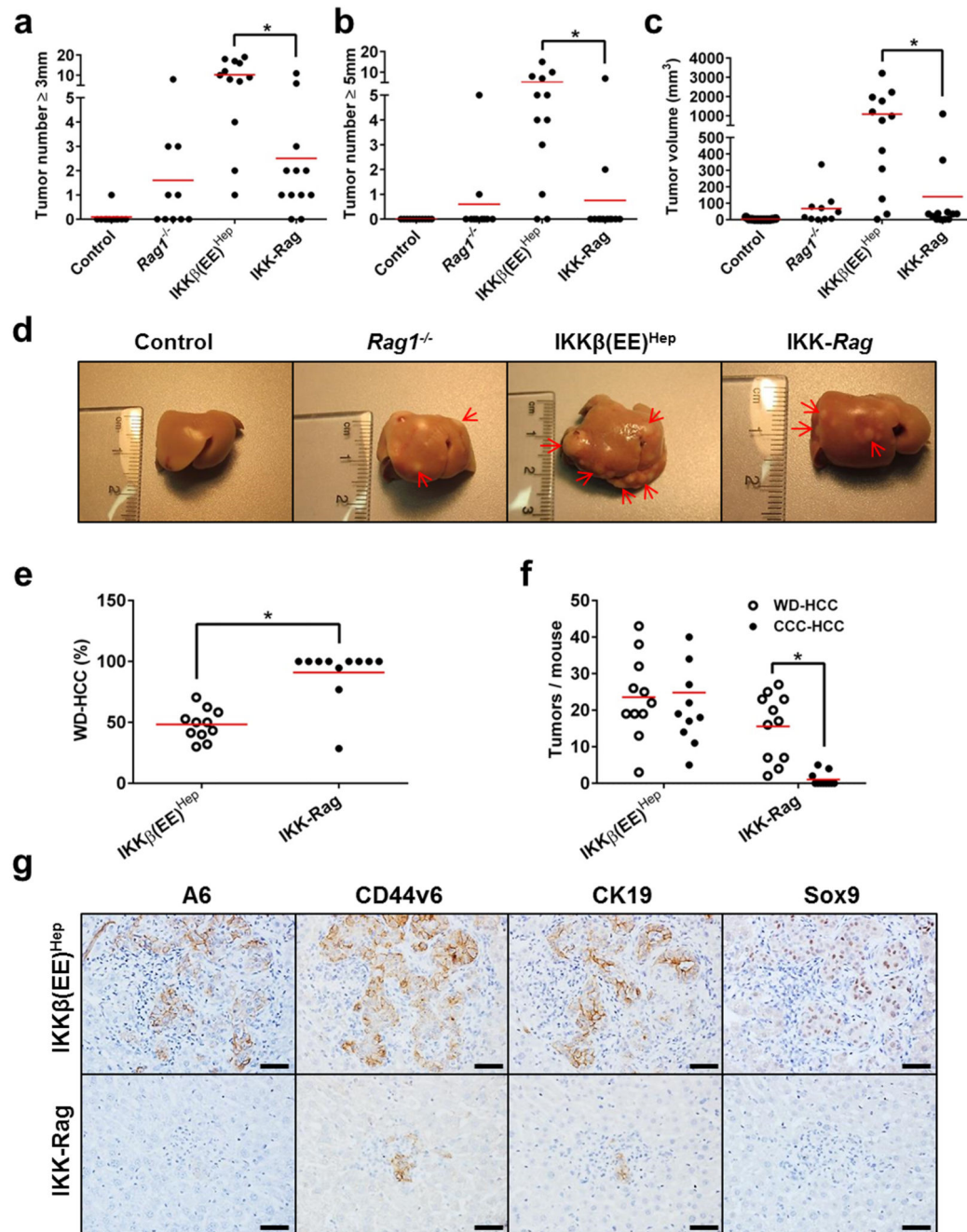


**Figure 5. Adaptive immune cells are required for ELS-dependent HCC promotion**

(a,b) Tumor numbers ( $\geq 3$  mm and  $\geq 5$  mm, respectively) and volume (c) in livers of 6 month old DEN-treated Alb-cre control, *Rag1*<sup>-/-</sup>, *IKK $\beta$ (EE)<sup>Hep</sup>* and *IKK $\beta$ (EE)<sup>Hep</sup> -Rag1*<sup>-/-</sup> (IKK-Rag) mice (n=11,10,12,12 for control, *Rag1*<sup>-/-</sup>, *IKK $\beta$ (EE)<sup>Hep</sup>* and IKK-Rag, respectively; \*p 0.006, two-tailed Students t-test; red line signifies mean). (d) Representative images of livers from 6-month-old DEN-treated mice. Arrows indicate tumors. (e,f) Tumor quantification by classification to well differentiated HCC (WD-HCC) or mixed cholangiohepatocellular carcinoma (HCC-CCC). n=11 for each group; \*p 0.00004, two-tailed

Students t-test; red line signifies mean. (g) Representative immunostains for the HCC progenitor markers A6, CD44v6, CK19 and Sox9 in 6 month old DEN-treated livers. HCC progenitors in  $IKK\beta(EE)^{Hep}$  liver are within ELSs, whereas the rare ones occasionally seen in  $IKK\beta(EE)^{Hep} - Rag1^{-/-}$  mice are in the parenchyma (scale bars- 50  $\mu$ m). Data are representative of one experiment, n=8.

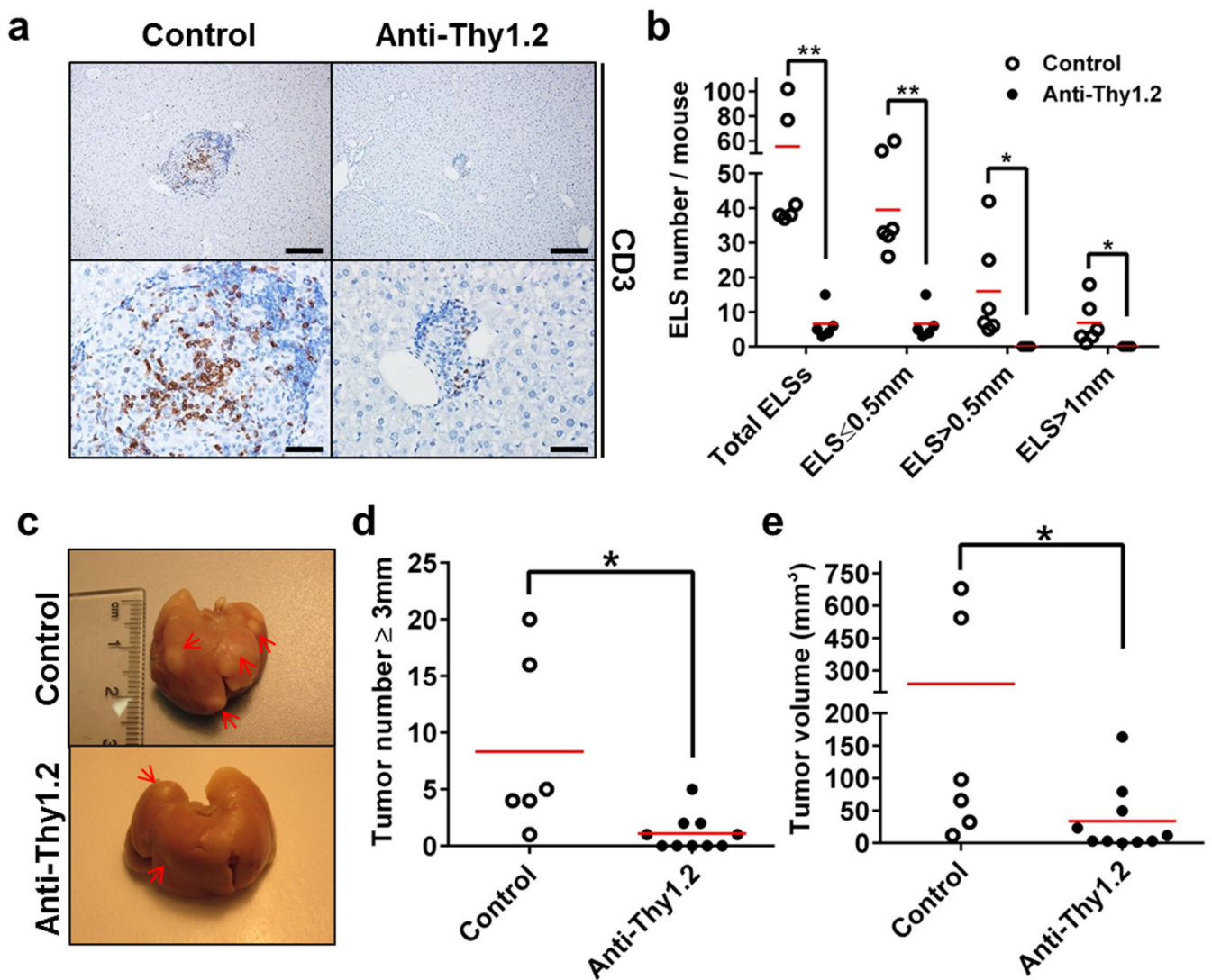


**Figure 6. Anti-Thy1.2 immuno-ablative treatment during ELS development attenuates liver tumorigenesis**

**(a)** Representative images of immunostaining for CD3 in livers from control or anti-Thy1.2 injected 6 months old DEN-treated  $\text{IKK}\beta(\text{EE})^{\text{Hep}}$  mice ( $n=6$ , scale bars upper 200  $\mu\text{m}$ , lower 50  $\mu\text{m}$ ). **(b)** Mice were treated with control or anti Thy1.2 antibody. Representative sections from the entire liver were assessed for the total number of ELSs and presence of ELSs of various sizes as indicated ( $n=6,5$  for control or anti-Thy1.2, respectively;  $*p < 0.04$ ,  $**p < 0.003$ , red line signifies mean) **(c)** Representative images of livers from control or anti-Thy1.2 injected 6-months-old DEN-treated  $\text{IKK}\beta(\text{EE})^{\text{Hep}}$  mice.  $n=6,10$  for control and anti-Thy1.2, respectively; arrows indicate tumors. **(d,e)** Tumor number ( $\geq 3$  mm) **(d)** and volume **(e)** in livers of control or anti-Thy1.2 injected 6-month-old DEN-treated  $\text{IKK}\beta(\text{EE})^{\text{Hep}}$  mice ( $n=6,10$  for control and anti-Thy1.2, respectively;  $*p < 0.04$ , two-tailed Students t-test, red line signifies mean). Data are representative of one experiment.

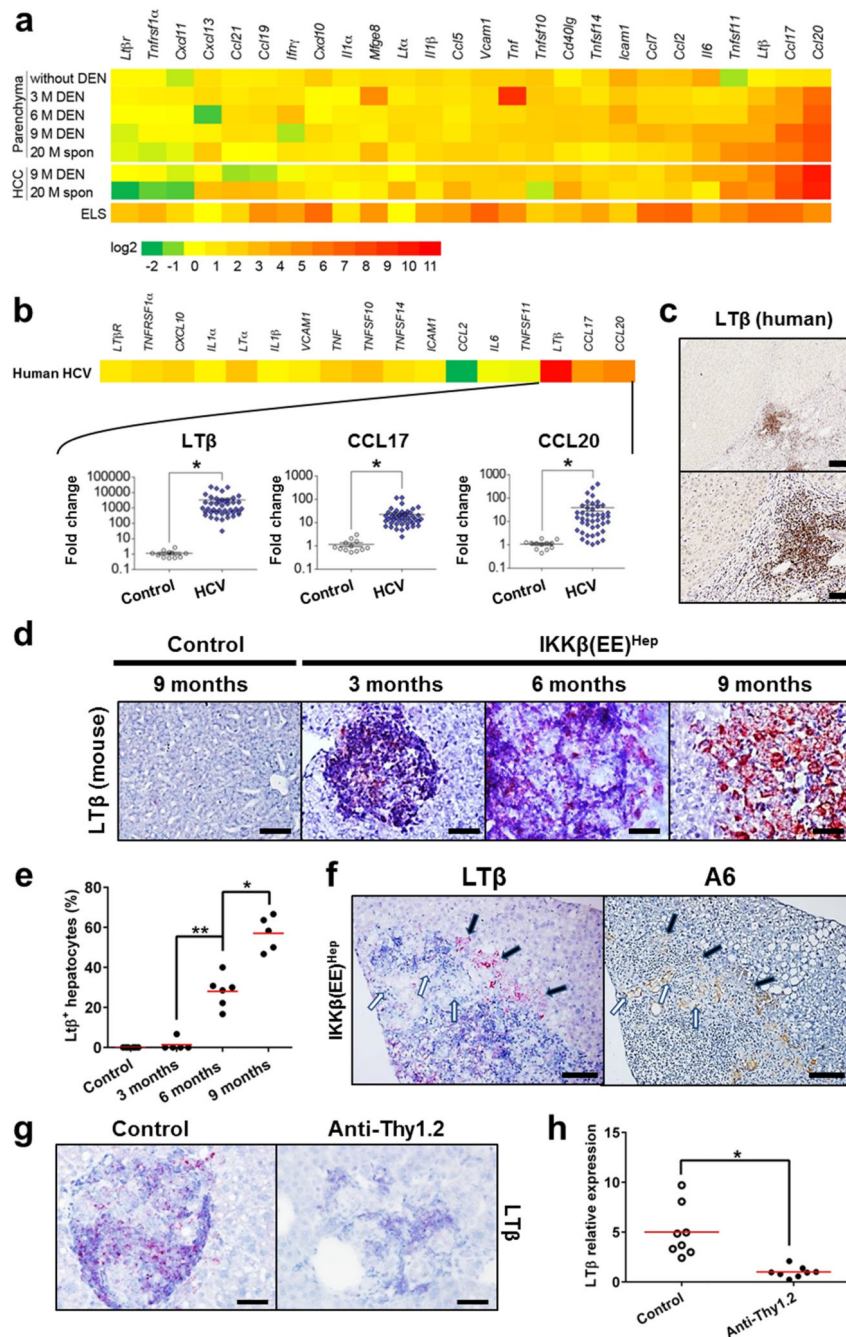


### Figure 7. ELS microniches provide a rich cytokine milieu

(a) mRNA qPCR analysis of liver parenchyma and HCCs from  $IKK\beta(EE)^{Hep}$  or DEN-treated  $IKK\beta(EE)^{Hep}$  mice (M=months of age), as well as in liver parenchyma of 3 month old  $IKK\beta(EE)^{Hep}$  mice without DEN treatment. Each data point reflects the median expression, normalized to the mean expression of the same gene in control livers derived from the equivalent Alb-cre control mice (for further details see Supplementary Tables 3, 4 & 5). (b) Heat map (upper) and scatter plot (lower) representations of mRNA qPCR analyses of liver tissue from HCV-infected patients (n=43) relative to healthy controls (n=12). Scatter

plots depict mRNA amounts of *LTβ*, *CCL17* and *CCL20* (for further details see Supplementary Tables 5 & 6; \* $p < 0.0001$ , two-tailed Students t-test,  $\text{Log}_{10}$  scale, cross line signifies mean). **(c)** Representative immunostaining for  $\text{LT}\beta$  in HCV-infected human liver (scale bars: upper 200  $\mu\text{m}$ ; lower 50  $\mu\text{m}$ ). **(d)** Representative *LTβ*-mRNA *in situ* hybridization in mouse livers (scale bars 50  $\mu\text{m}$ ). **(e)** Quantification of  $\text{LT}\beta$  expression in malignant hepatocytes. The % of  $\text{LT}\beta$  positive hepatocytes was determined by counting 10 ELSs from each mouse ( $n=8,5,6,5$  for control, 3, 6 and 9 months old mice, respectively; \* $p=0.0003$ , \*\* $p=0.00006$ , two-tailed Students t-test, red line signifies mean). **(f)** Representative serial sections showing  $\text{LT}\beta$  mRNA in-situ hybridization and immunostaining for the progenitor marker A6. Note  $\text{LT}\beta$  staining of immune cells and egressing hepatocytes (black arrows) but not niche residing ones (white arrows, scale bars-100  $\mu\text{m}$ ). **(g)** Representative images of *LTβ*-mRNA in-situ hybridization in hepatic ELSs of control or anti-Thy1.2 injected 6 month old DEN-treated  $\text{IKK}\beta(\text{EE})^{\text{Hep}}$  mice (scale bars-50  $\mu\text{m}$ ). **(h)** qPCR analysis of *LTβ* mRNA expression in liver parenchyma of control or anti-Thy1.2 injected 6 month old DEN-treated  $\text{IKK}\beta(\text{EE})^{\text{Hep}}$  mice ( $n=10,6$  respectively; \* $p=0.003$  two-tailed Students t-test, red line signifies mean). Data are representative of one experiment in (a) and (b) and of two independent experiments in (c), (d), (f) and (g).

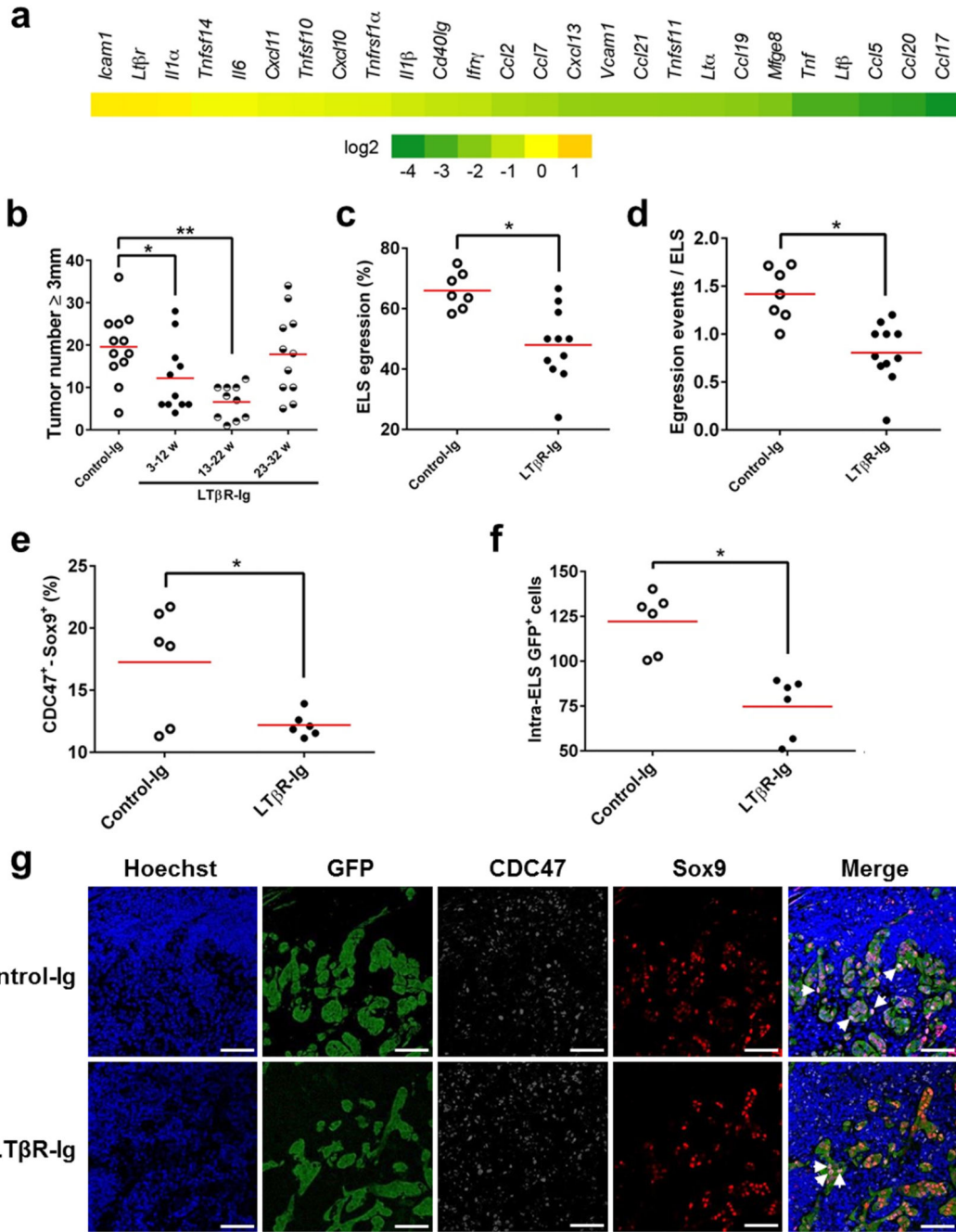


**Figure 8. Blocking LT signaling abolishes microniche egression and tumorigenesis**  
**(a)** Heat map representation of mRNA qPCR analysis of liver parenchyma from 33-week-old  $\text{IKK}\beta(\text{EE})^{\text{Hep}}$  mice treated with LTβR-Ig for 10 consecutive weeks (23-32 weeks, see Supplementary Fig. 8a). Each data point reflects the median expression, normalized to the mean expression of the same gene in equivalent control murine-IgG1-injected  $\text{IKK}\beta(\text{EE})^{\text{Hep}}$  mice ( $\text{Log}_2$  scale; See Supplementary Tables 4 & 5). **(b)** Tumor number ( $> 0.5$  cm) in livers of 33 week old  $\text{IKK}\beta(\text{EE})^{\text{Hep}}$  mice treated with either control-Ig or LTβR-Ig for the indicated periods (n=12,11,10,11 for control, 3-12w, 13-22w or 23-32w, respectively;



\* $p=0.04$ , \*\* $p=0.0002$ , two-tailed Students t-test, red line signifies mean). **(c,d)** Quantification of the percent of ELSs showing egressed progenitor hepatocytes **(c)** and of the number of egressing hepatocyte clusters per ELS **(d)** [ $n=7,11$  for control-Ig and LT $\beta$ R-Ig treated mice, respectively; \* $p=0.02$ , and 0.00009 for **(c)** and **(d)**, respectively; two-tailed Students t-test, red line signifies mean]. **(e)** Quantification of the CDC47<sup>+</sup>Sox9<sup>+</sup> double positive cells in ELSs (see below, pink in **g**, right panels) ( $n=6$ ; \* $p=0.02$ , two-tailed Students t-test, red line signifies mean). **(f)** Quantification of the GFP<sup>+</sup> cells inside the ELSs ( $n=6$ ; \* $p=0.001$ , two-tailed Students t-test, red line signifies mean). **(g)** Representative confocal microscopy images of ELS-containing liver sections from DEN-treated IKK $\beta$ (EE)<sup>Hep</sup> mice injected for 10 consecutive weeks (23-32 weeks) with control-Ig or LT $\beta$ R-Ig for GFP, CDC47 and Sox9. Hoechst 33342 marks the nuclei. Arrows indicate CDC47<sup>+</sup>Sox9<sup>+</sup> double positive cells in pink (scale bars 100  $\mu$ m). Data are representative of one experiment in **(a)** and **(b)** and of two independent experiments in **(g)**.